# ERS-2 Scatterometer: Mission Performances and Current Reprocessing Achievements

Raffaele Crapolicchio, Giovanna De Chiara, Anis Elyouncha, Pascal Lecomte, Xavier Neyt,
Alessandra Paciucci, and Marco Talone, *Member, IEEE*

*Abstract*—This paper presents an overview of the evolution of the European Remote-sensing Satellite (ERS)-2 scatterometer mission during the last 16 years, highlighting the changes in both satellite configuration and on-ground data processing algorithm. Instrument and on-ground data processor performances and evolutions are analyzed and commented; finally, future developments are emphasized. ERS-2 was launched in 1995 by the European Space Agency (ESA). Since then, the active microwave instrument, which is one of the ERS-2 payloads, is providing radar backscattering coefficient measurements by using its three nominal operational acquisition mode: synthetic aperture mode (SAR mode), scatterometer mode (wind mode), and a special combination of the two over ocean where SAR and scatterometer mode are interleaved (wind/wave mode). The main applications for data acquired in scatterometer mode are related to the estimation of the wind vector over the sea surface. In that field, the ERS-2 scatterometer measurements give a very valuable contribution to the accuracy of the numerical weather forecast models, being assimilated in several meteorological weather forecast centers since the beginning of the mission. Other applications of the ERS-2 scatterometer data are over land to retrieve information about the soil water content and over the sea-ice. A constant monitoring of the scatterometer performances is carried out since the beginning of the mission by ESA engineering teams located in ESTEC and ESRIN and the instrument manufacture (Dornier at launch time), in collaboration with several European research institutions, as the European Centre for Medium-range Weather Forecasts for product geophysical validation, the Belgian Royal Military Academy for data processing and calibration during the zero-gyro phase, and industrial partners, as Serco SpA for the routine data quality control activities since the beginning of operational phase. Results show outstanding performances even after the failure of several hardware components that has been properly compensated on-ground with evolution of the processor, and many years of operation, which permits the creation of a homogeneous database of wind vectors for the last 16 years (20 years if the ERS-1 mission is considered), in accordance with Global Climate Observing System recommendations.

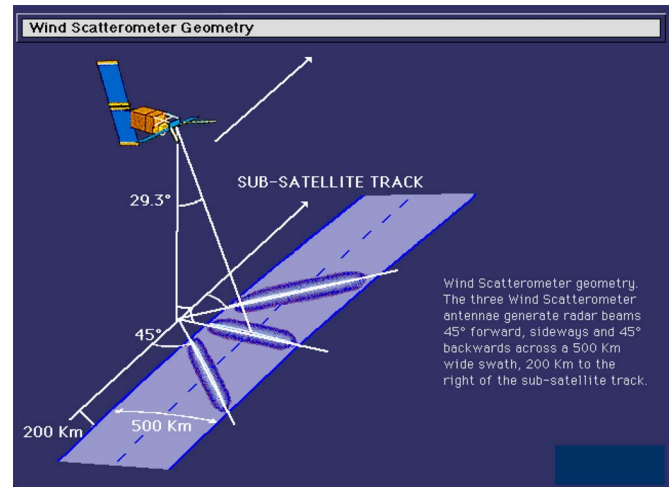*Index Terms*—Calibration, C-band, European Remote-sensing Satellite (ERS), scatterometry, wind vector.

Fig. 1. ERS-2 scatterometer geometry and its field of view.

## I. INTRODUCTION

THE EUROPEAN Remote-sensing Satellite (ERS)-2 [1] was launched in July 1995 as the follow-on mission to ERS-1. It embarks six different instruments, namely a radar altimeter working in the Ku-band (13.8 GHz), the along-track scanning radiometer (infrared and microwave), an ultraviolet and visible spectrometer called global ozone monitoring experiment, a microwave radiometer (acquiring at 23.8 and 36.5 GHz), an active microwave instrument (AMI) working at 5.3 GHz (C-band). AMI can be operated in three different acquisition modes, namely:

— the synthetic aperture radar (SAR) image mode, whose output are 100 km-wide strips of high-resolution imagery.
— the SAR wave mode, which produces 5 km × 5 km images ("imagettes") at intervals of 200 km along track.
— the wind scatterometer mode, which provides measurements of radar backscatter from the sea surface.

The ERS-2 wind scatterometer [2] consists of three different antennas looking at 45° forward, sideways, and 45° afterward with respect to the satellite's flight direction. The resulting swath is 500 km wide and is centered 450 km at the right of the satellite's nadir; the nominal spatial resolution of the ERS-2 wind scatterometer is 50 km, each resolved point at the Earth is called node. The geometry of the instrument and its field of view are shown in Fig. 1.

The ERS-2 scatterometer measures the so-called radar cross-section $\sigma^0$ of the Earth surface, which is, on the sea, directly

connected to the sea roughness. The sea roughness is coupled with the surface wind speed (it increases when the wind speed increases). The most widely used forward models relating $\sigma^0$ to the wind speed are empirical and are periodically updated and improved based on real satellite measurements. Within this context, the calibration and performance monitoring of the sensor plays a fundamental role. More importance to the continuous performance monitoring has been given in 2003 by the Global Climate Observing System (GCOS) Steering Committee, which identified the wind speed and direction as two of the essential climate variables (ECVs). ECVs are important descriptors of the evolution of the global climate and the creation of homogenous, long and global databases of those is strongly encouraged by GCOS.

The European Space Agency (ESA), in collaboration with the European Centre for Medium-range Weather Forecasts (ECMWF), the Belgian Royal Military Academy (RMA), and Serco SpA, provides regular quality monitoring reports for ERS-2 since the beginning of the mission.

In this paper, the description of the data processing algorithm, including its future improvements, is given in Section II. A short summary of the satellite performance evolution, in terms of main mission events and instrument performance is presented in Section III. In Section IV, an overview of the different calibration techniques applied to ERS-2 data is given. Finally, Section V is devoted to the definition of a homogeneous wind vectors database comprehending the whole mission and the cross-calibration plan with ERS-1.

## II. DATA PROCESSING

### A. Main Events

Scatterometers and the associated data processing are radar systems designed to provide a measurement of the Earth-surface backscatter $\sigma^0$ (sigma naught) with an extreme precision and stability.

The overall processing is described in [2] and [3] and can be summarized as follows. The instrument transmits sequences of 32 radio frequency (RF) rectangular pulses and the corresponding echoes are digitized, recorded, and transmitted to the ground. On ground, the nonlinearities of the analog-to-digital converter (ADC) are corrected for, particularly for low-amplitude signals. Next, a correction filter is applied to correct for the transmittance of the on-board analog anti-aliasing filter. The residual Doppler frequency shift is then removed before a final adjustment of the bandwidth of the signal. The echo power of each of the 32 pulses is then averaged together in each range bin in order to reduce speckle and the noise power is subtracted to yield the echo power at full resolution.

Calibrated measurements are obtained by inverting the radar equation to yield the calibrated $\sigma^0$ at full resolution

$$\sigma^0 = \frac{(4\pi)^3 R^3}{\lambda^2 G^2} \frac{P_R}{P_T} \qquad (1)$$

where $R$ is the distance between emitter and target, $\lambda$ the used wavelength, $G$ the antenna gain, and finally $P_R$ and $P_T$ the received and emitted power, respectively. As can be deduced by (1), atmospheric losses are not considered: no terms are included depending on atmosphere status and condition. At C-band, in fact, atmosphere can be considered transparent and can be neglected as well as rain events.

One of the key parameters in this inversion is an accurate measurement of the transmitted power, that can fluctuate both in the short term, e.g., after instrument power-up and in the long-term due to aging of the high power amplifier (HPA). Another key parameter is the gain of the antenna in elevation. One of the main focuses of the calibration described in Section IV is an assessment of the antenna diagram and its possible evolution in time.

One of the main issues is the reduction of the speckle, the random variations of the measurement inherent to the coherent nature of the radio waves used. The averaging of the power of the 32 echoes per range bin is a first step. After calibration, the raw-resolution $\sigma^0$ are further spatially averaged to match the specified spatial resolution of the instrument and further reduce the variance of the obtained measurement. It can be shown that averaging the power of statistically independent and identically distributed samples indeed provides the maximum likelihood estimate of the backscattering coefficient.

### B. Yaw Angle Measurement

In nominal operation, the satellite is piloted in the so-called yaw steering mode (YSM) where the side-looking midantenna is pointed orthogonal to the satellite ground track. The goal of this piloting is to guarantee as much as possible that the echo signal will have a zero Doppler frequency. A Doppler frequency shift due to the orientation of the antenna is inevitable for the fore and aft antennas. This range-varying Doppler frequency shift is partially compensated for on-board. The YSM and the on-board compensation are essential to guarantee that the received signal will fit in the pass-band of the ADC (30 kHz). The spectrum of the transmitted square pulse is cardinal-sine shaped and a monitoring of the shape and center (the Center of Gravity (CoG) of the spectrum) provides an easy way to monitor the accuracy of the pointing and of the on-board Doppler frequency compensation.

After failure of the on-board gyroscopes, the satellite was piloted in zero-gyro mode (see Section III), and this resulted in a degraded attitude. The attitude and particularly the yaw angle of the satellite have to be estimated on the one hand to correctly position the measured samples on the ground and on the other hand to correctly compensate for the Doppler frequency shift induced by a nonzero yaw error angle. The attitude can actually be obtained by determining the Doppler frequency shift. This is performed by assessing the spectral location of the cardinal sine of the echoes. This assessment is performed by fitting a Gaussian model to the spectrum of the echo signal estimated over the 32 pulses [3]. To take into account the inertia of the satellite and to filter out geophysical effects, along-track averaging of the estimated yaw angle is performed.

### C. Evolution of the Ground Processing

The initial processor (Stand-alone—Low bit Rate Data Processing Facility, S-LRDPF) developed prior to the launch of

TABLE I
ERS-2 SCATTEROMETER PRODUCTS OVERVIEW

| Product Description | TOSCA Prototype Processor (on demand processing only for Cal/val users) | ASPS Operational Processing (all users) |
|---|---|---|
| **ASPS L1.0** Calibrated and geolocated $\sigma_0$ at raw resolution (echo samples) | yes | no |
| **ASPS L2.0 nominal resolution** Calibrated sigma nought + Wind Field vector and Ice probability geolocated with 50Km spatial resolution | yes | yes |
| **ASPS L2.0 high resolution** Calibrated sigma nought + Wind Field vector and Ice probability geolocated with 25Km spatial resolution | yes | yes |
| **ASPS L2.0 User Defined Grid** Calibrated sigma nought + Wind Field vector and Ice probability geolocated with a user-defined resolution | yes | no |

the satellite has been reviewed in 2001. The main focus of this review was to be able to handle data acquired in degraded attitude. Indeed, the initial processor relied on precomputed tables computed for a nominal attitude along the nominal orbit. There were essentially two tables: the calibration factor table and the node-appurtenance table. The calibration factor table took into account all the geometric factors (including antenna pattern) appearing in the radar equation and was used to convert power measurements to $\sigma^0$. The node-appurtenance table was used to assign raw measurements to a particular node in the spatial averaging process. In a situation where the attitude is not precisely known in advance, precomputed tables are useless. The second focus of the review was a general modernization of the processing [3] made possible due to the higher available processing power on ground. In addition, in the on-the-fly estimation of the yaw angle and subsequent computation of the correct geometry and Doppler frequency shift compensation, the processing also implies the displacement of the compensation of the ADC nonlinearity before any linear operation on the signal and an anti-aliasing filter correction using a Wiener filter able to take into account the displacement of the spectrum of the received signal.

### D. Fixed Grid Product

As part of the processor review, new output products were specified. In addition to the nominal resolution product (50 km), a high-resolution product (25 km) and a raw-resolution product were defined. These are only available on reprocessed data.

In the current ERS wind product (and most scatterometers), the nodes are defined relative to the satellite ground track, i.e., the lines of nodes are orthogonal to the satellite ground track, the center node of the swath is at a constant elevation angle seen from the satellite (what implies that the nodes sways cross-track as the altitude of the satellite evolves along the orbit) and the along-track node spacing is synchronized to the along-track sampling of the raw measurements.

In order to assure the uniformity of all the scatterometer data, a new scatterometer product is introduced. In the new product, the nodes are defined on an Earth fixed grid rather than the usual satellite swath related grid. This product will make easier a comparison of level 2 data given different scatterometers, or in general between different remote sensing instruments. Therefore, geophysical parameters (wind field, soil moisture ...) can be intercompared between different platforms (ERS-2, METOP, SMOS ...), regardless of their distinct configuration and geometry of acquisition thus avoiding resampling and interpolation operations that may introduce approximations.

The approach of a fixed grid product is based on the definition of the nodes from a predefined discrete global grid which is independent of the satellite swath. A number of grids have been analyzed [4] for the following characteristics: conformality, isotropy, global coverage, adjacency, and the minimization of the intercell distance variation. The Icosahedron Snyder Equal Area (ISEA) partitioned with hexagons at aperture 4 resolution 9 (ISEA4H9) presents uniform adjacency with a mean intercell distance of 15.072 km and a standard deviation of 0.9 km [5]. Therefore, this grid was chosen for the processing of SMOS level 1C data. For the characteristics listed above and for compatibility with SMOS, the same grid is used for this new product.

The current (for both the original S-LRDPF processor and the revised ERS Scatterometer Attitude Corrected Algorithm (ESACA) / Advance Scatterometer Processing System (ASPS) processors) spatial filtering consists mainly in a weighted integration of samples belonging to an area around each node [2]. The weighting function used is a 2-D separable Hamming window with axis parallel to the along and across-track directions in order to meet the spatial resolution specifications. In the new approach (ISEA4H9 grid), the spatial sampling is hexagonal. In order to achieve a higher resolution compatible with the considered sampling, the spatial averaging window consists in a radial Hamming window in which the window length in the along and across track direction differ in order to cope with the differing pre-existing spatial filtering inherent to the instrument

respectively due to the azimuth antenna diagram, and the pulse length.

A summary of the available products for the ERS-2 scatterometer, including both nominal processing and reprocessing, is shown in Table I, where TOSCA stands for TOol for Scatterometer CAlibration.

## III. MISSION PERFORMANCE

Since 1995, three key parameters have been selected to monitor the ERS-2 scatterometer long loop performance; these are regularly recorded at ESA's facility using ERS-2 level 1 data product. Namely, the *internal calibration pulse power*, the *received signal spectrum* (in terms of CoG and its standard deviation), and *noise power* for both in-phase (I) and quadrature (Q) channels are checked. Hardware failures, changes in the configuration, as well as nominal instrumental drifts determined the evolution of these three parameters, which, in turns, triggered corrective actions, acting thus as both trackers and drivers of the instrument performances.

A summary of the main events that affected ERS-2 satellite is presented in the following paragraph, their impact on the instrument performances is, instead, assessed in Sections III-B–E.

### A. Main Events

The most important changes in the satellite flight and ground segments are listed below and shown in Fig. 2, where the events are chronologically listed between the two time bars, and their effects on the flight and ground segment are presented in the left and right time bars, respectively; the small bar on the extreme right shows the change in data processor at the ground segment.

*1995, Apr.*—ERS-2 is launched on April 21, 1995 from ESA's Guiana Space Centre near Kourou, French Guiana.

*1995, Nov.*—After some technical problems, the first scatterometer measurement is achieved.

*1996, Aug.*—Due to an anomaly in the internal calibration unit, the calibration subsystem is switched from side A (nominal) to side B (redundant).

*2000, Jan.*—Operation mode is changed from nominal to mono-gyro mode. Three of the six on-board gyroscopes, namely gyro 1, 2, and 5 fail, corresponding to the $x$-direction (1 and 2) and the $z$-direction (5). In mono-gyro configuration the accuracy of the satellite attitude was degraded in particular for the yaw angle. Due to the consequent measurement quality degradation, data distribution, and assimilation by ECMWF is firstly discontinuous and then interrupted. ESA started a fully review of the scatterometer processor in cooperation with RMA to compensate for the degraded attitude and recovery the scatterometer mission.

*2001, Jan.*—Other two gyroscopes fail (gyros 3 and 6, corresponding to the $y$- and $z$-directions), leading to the so-called zero-gyro mode; the single (gyro 4) operating gyroscope is only used for important orbital maneuvers.

*2001, Jun.*—To test a way to compensate for the gyroscopes failure, ERS-2 satellite starts operating only in wind-wave acquisition mode.
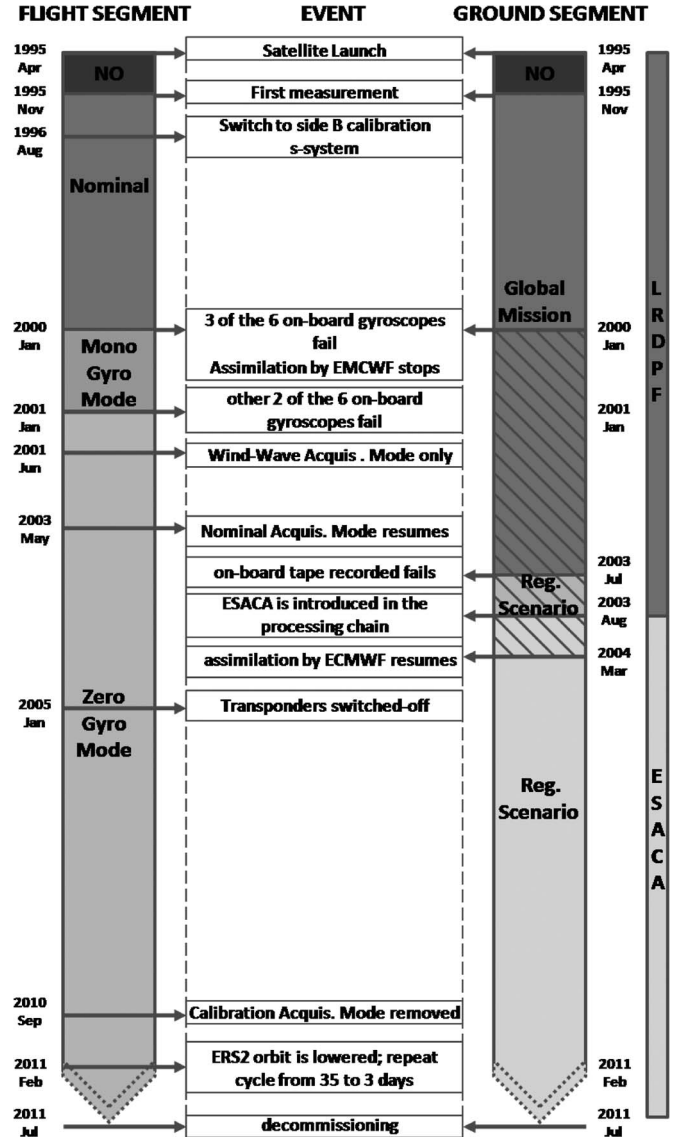


Fig. 2. (Between the time bars) main events that affected ERS-2 satellite, and their effects on (left time bar) flight and (right time bar) ground segment. The small bar on the extreme right shows the change in data processor at the ground segment.

*2001, Jun.*—Positioner failed for the transponder in Adra. Only one transponder in El Arenosillo is operational.

*2003, May.*—Nominal acquisition mode is resumed.

*2003, Jul.*—The on-board tape recorded fails, since then, data are available only when the satellite is within the visibility of some ground station; the mission passes from Global to Regional coverage.

*2003, Aug.*—ESACA is included in the processing chain to compensate for the switching off of the gyroscopes. Following the success of the ESACA algorithm ESA starts to increase the number of acquisition stations and to deploy the ESACA processor to improve the coverage of scatterometer data for the regional mission scenario. At the end of ERS-2 mission in 2011, the following acquisition and processing station are operative: Beijing (CN), Chetumal (MX), Cuiaba (BR) (not available in real-time), Gatineau (CDN), Hobart (AUS), Kiruna (S),

Maspalomas (E), Matera (I), McMurdo (Antarctica), Miami (U.S.), Singapore, and West Freugh (U.K.).

*2004, Mar.*—Assimilation of ERS-2 scatterometer data by ECMWF is resumed.

*2005, Jan.*—Due to a system failure (power supplies broke down), the acquisition using the remaining transponder at El Arenosillo is been discontinued.

*2010, Sep.*—Since the impossibility of the transponder repair, the calibration acquisition mode is removed from the orbital planning and substituted by nominal acquisition.

*2011, Feb.*—ERS-2 is lowered by a series of orbit maneuvers. As a consequence of that, the repeat cycle changes from 35 to the 3 day.

*2011, Jul.*—ERS-2 decommissioning and de-orbiting is foreseen.

Further details are given in the following paragraphs, where the definitions of the three checked parameter are given, and any of the aforementioned events is commented in relation with its effect on the instrument performances.

## B. Internal Calibration Pulse Power

As stated in Section II, the normalized radar cross section is defined as in (2), repeated here for convenience

$$\sigma^0 = \frac{(4\pi)^3 R^3}{\lambda^2 G^2} \frac{P_R}{P_T} \qquad (2)$$

where $R$ is the distance between emitter and target, $\lambda$ the used wavelength, $G$ the antenna gain, and finally $P_R$ and $P_T$ the received and emitted power, respectively. From (2) the importance of a correctly calibrated emission and reception chains is evident: any loss and drift of the system must be measured and taken into account to guarantee the proper measurement of $\sigma_0$.

The transmit pulse is produced at the intermediate frequency, amplified, upconverted to RF, and amplified again by the HPA before being routed toward the antennas. The path for the received pulse is contrary, with the received echo routed to the low noise amplifier of the receiver. The internal calibration pulse power is a replica of the transmitted pulse injected into the receiver by the calibration subsystem. It is used to calibrate the received echo as per (2) and is regularly monitored to assess the performance of both the transmitter and receiver chains. In Fig. 3, the evolution of the daily (solid line) averaged internal calibration pulse power and (dashed line) its standard deviation are shown for the fore, mid, and aft antennas since the beginning of scatterometer operations in November 1995.

As can be noticed, the internal calibration pulse power has been decreasing since the beginning of the mission; Corrective actions have been taken to keep it in the correct dynamic range with the received echo and allow a proper retrieval of the wind vector. The pulse power was increased in 1998, 2002, and 2009, while an increase of the receiver gain caused the rise recorded in 2003.

## C. Centre of Gravity (CoG) and Its Standard Deviation

Due to the relative motion between the satellite and the target, the radar echo emitted by the Earth surface does not have the same frequency for all the observed nodes. This frequency shift is much larger for the side antennas (50–150 kHz) than for the mid one ($\pm 10$ kHz). To compensate for that shift, satellite yaw is continuously modified as well as the central frequency of the scatterometer receiver. The receiver signal spectrum CoG and its standard deviation monitor the orbit stability and the performances of the Doppler compensation filter (on-board and on-ground compensation). In Fig. 4, the evolution of the (solid line) daily averaged Doppler Compensation and (dashed line) its standard deviation are shown, as for Fig. 3, for the fore, mid, and aft antennas since the beginning of the scatterometer operations.

The very large fluctuations in Fig. 4, between January 2000 and August 2003, are due to the failure of the on-board gyroscopes, and the consequent implementation of the mono and zero-gyro modes. The nominal performance is resumed with the introduction of ESACA in the processing chain.

## D. Noise Power for Both Q and I Channels

Noise power is another very important parameter to be estimated and monitored. Any received echo is affected by noise, and this must be subtracted to obtain the noise-free backscatter. Noise power on both Q and I channels is constantly recorded and sent to the ground stations for the correction. These are shown in Fig. 5, in terms of the evolution of their daily average for the fore, mid, and aft antennas since the beginning of the scatterometer operations in November 1995. As can be noticed in Fig. 5, the noise power is stable around 1 ADC unit for the fore and aft antennas (approximately 2 ADC after February 2003), while the midantenna noise power is very low and not measurable. The different noise level for the midbeam with respect to the fore and aft beams, theoretically not expected, can be ascribed to the fact that the noise level is measured at the end of the receiver chain, which is not exactly the same for the different beams.

The high peaks detected between December 1997 and November 1998 are due to the presence of corrupted values in the noise measurements. The increase of the noise power on February 2003 is, instead, due to the increase of the receiver gain, modified to optimize the signal dynamic at the input of the A/D Converter.

## E. Stability of the Satellite Attitude

During the nominal mode and the mono-gyro mode (until January 2001), the stability of the satellite attitude was assured by the six (three during the mono-gyro mode) on-board gyroscopes. Since January 2001, and until August 2003, between the entrance in the zero-gyro Mode and the introduction of ESACA in the processing chain, satellite attitude was not guaranteed, in particular for the yaw angle, causing the high fluctuation in the received echo's spectrum as shown in Fig. 4. ESACA processor, analyzing the spectrum of the received echo, computes the error on the yaw angle estimation and compensate for that the final calibrated sigma noughts. The computation of the yaw error angle is done assuming a negligible errors for the roll and pitch angles. This assumption
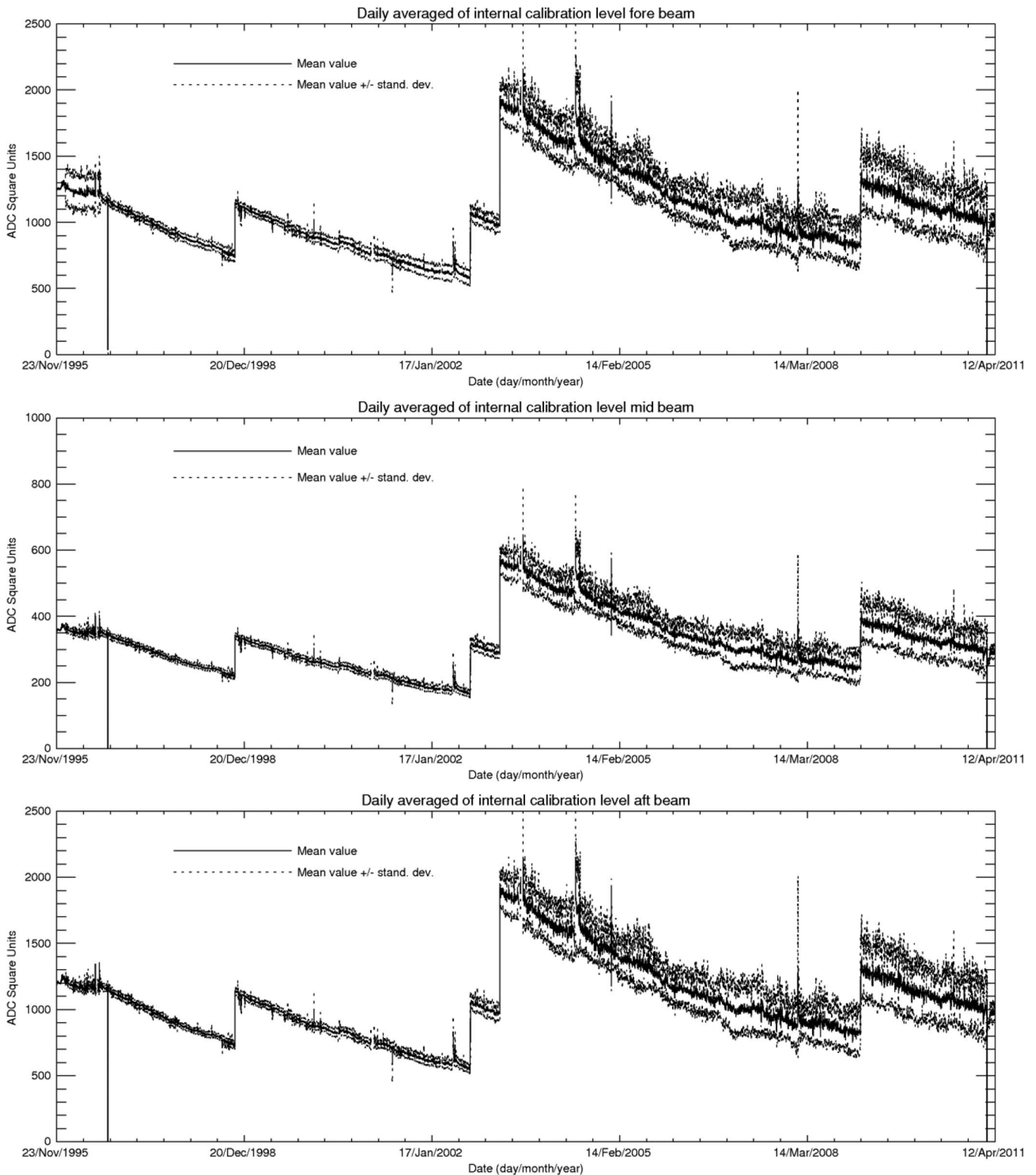
Fig. 3. Evolution of the daily (solid line) averaged internal calibration power and its (dashed line) standard deviation is shown for the fore, mid, and aft antenna since the beginning of scatterometer operations in November 1995.

has been verified during the zero-gyro mode commissioning phase using inputs data from other on-board sensors, mainly the radar altimeter for the pitch error and the SAR instrument for the roll.

The effectiveness of the ESACA processor is clearly shown in Fig. 4, where the received echo spectrum fluctuation was returned to the nominal range after the deployment of the ESACA processor in the ground segment. ESACA processor also generates a dedicated product (the HElpful Yaw, HEY, product), which is used to monitor and control the stability of the satellite attitude. Yaw information is regularly sent to the flight segment to correct the satellite attitude. Since 2003,
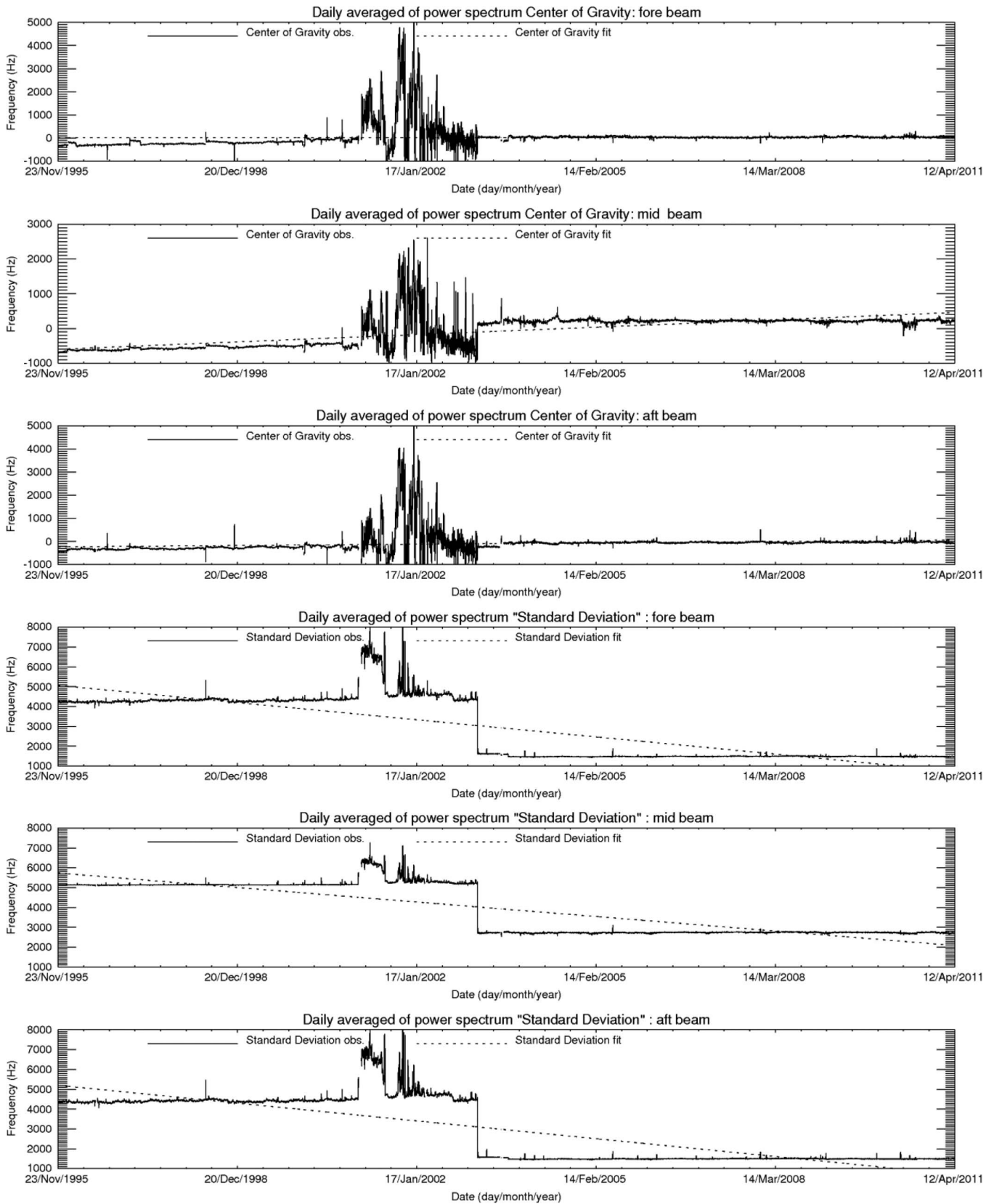
Fig. 4. Evolution of the (solid line) daily averaged center of gravity and (dashed line) its standard deviation is shown for the fore, mid, and aft antenna since the beginning of scatterometer operations in November 1995.

the yaw angle, as estimated using the HEY files, is regularly recorded; the different steps of the satellite yaw monitoring are shown in Fig. 6.

The estimation of the yaw error angle is based on the Doppler shift measured on the received echo (first three plots for the fore, mid, and aft antenna) and aims at computing the
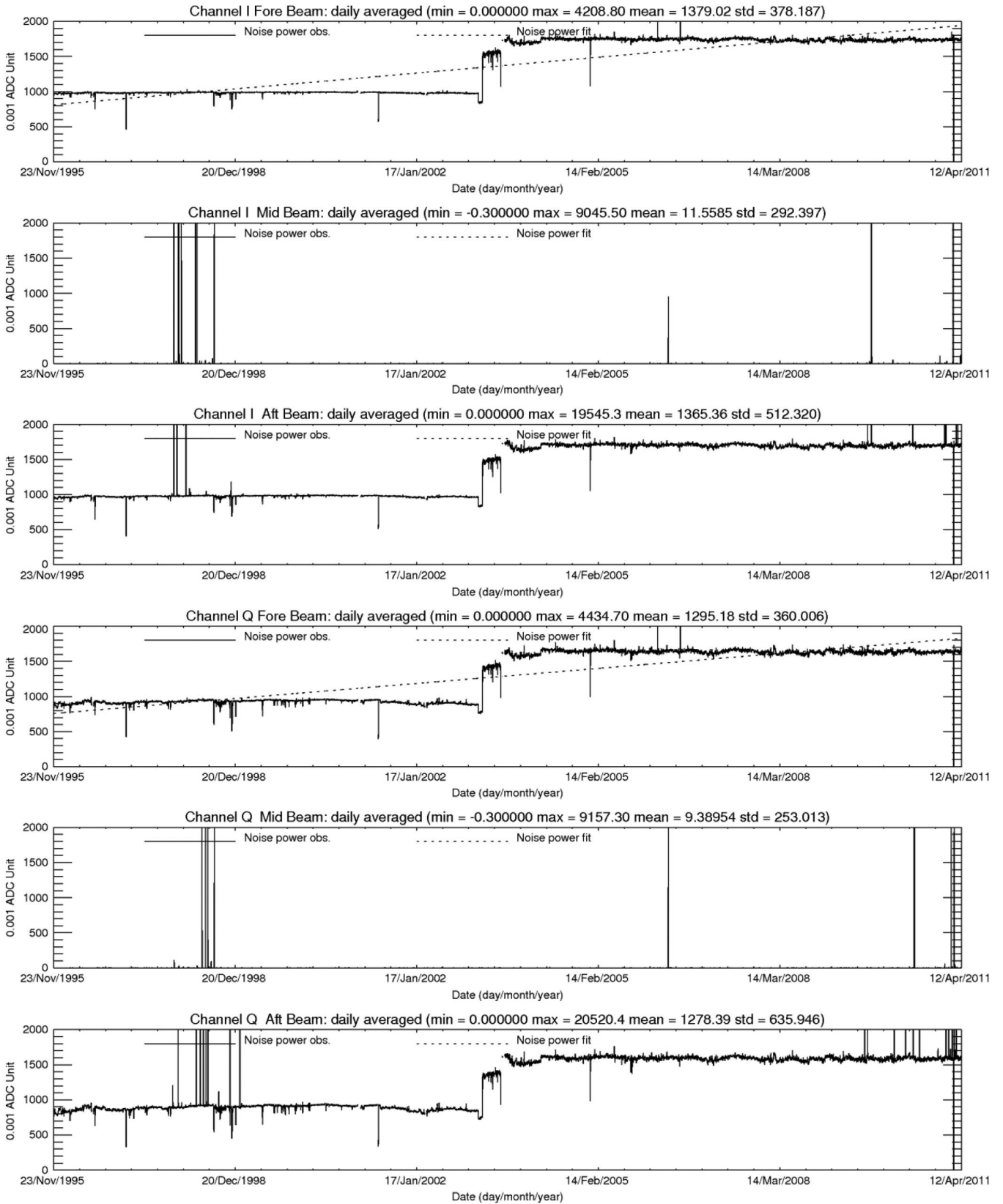
Fig. 5. Evolution of the in-phase (I) and quadrature (Q) noise power for the fore, mid, and aft antenna since the beginning of scatterometer operations in November 1995.

correct acquisition geometry for the three scatterometer antennas throughout the entire orbit. The yaw error angle information is used to compensate for the additional Doppler frequency shift

due to the yaw error angle and to position the echo samples at their correct location on the ground before being associated to each node in the spatial filter. The result of the monitoring
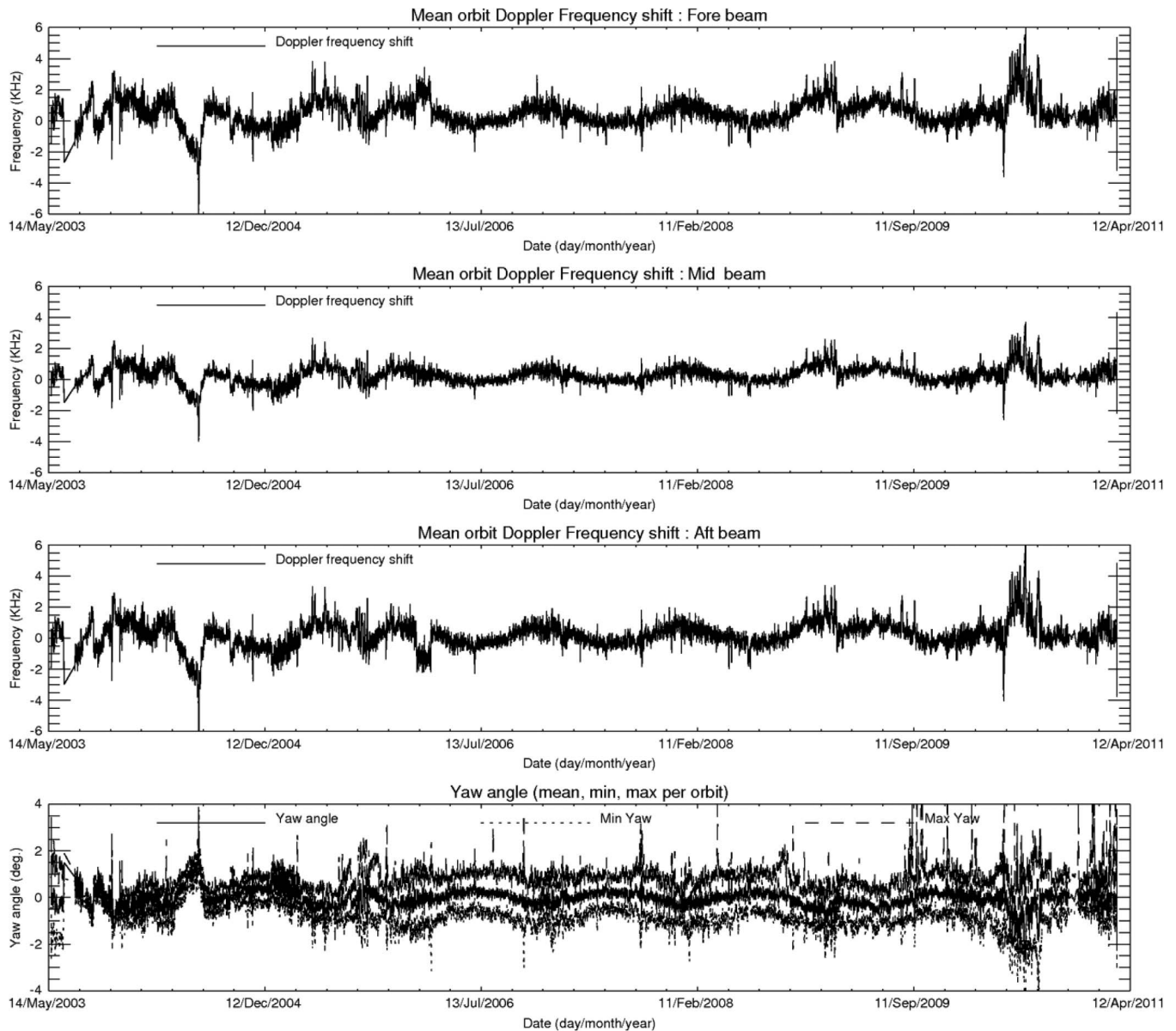
Fig. 6. Satellite's yaw monitoring.

(fourth plot) is a yaw error angle within $\pm 2$ deg. for most of the orbits. That value is within the specification for the ESACA processor to assure calibrated data.

## IV. CALIBRATION MONITORING

Apart for all the internal calibration procedures, external calibrations techniques have been defined to monitor the instrument performance. Two main parameters have to be assessed: the absolute calibration, permitting an evaluation of the stability of the instrument in the long term, and a relative calibration, essentially aiming at validating the elevation antenna pattern of the instrument scatterometer.

The only way to perform absolute calibration consists in using active transponders measurements. The calibration procedure using transponders is not reported in this paper because

considered out of the scope, a detailed description of this can be found in [6]. Apart from the absolute calibration, distributed targets may be used to perform an assessment of the elevation antenna pattern more rapidly than using transponders. The tropical rain forest in South America has been used since the beginning of the mission as a reference distributed target by the Product Control Service (PCS), after the switch to Regional Scenario, and the consequent lack of coverage of the Rain Forest, alternative calibration targets have been used, as Polar Regions or the ocean surface. In addition to that, cross-calibration with ASCAT was also tested. These will be presented in the following paragraphs. It is worth to stress on the fact that all the presented targets, namely rain forest, Polar Regions, and ocean surface, have been used, in the nominal processing, only for monitoring purposes and have no impact on the sensor calibration itself.
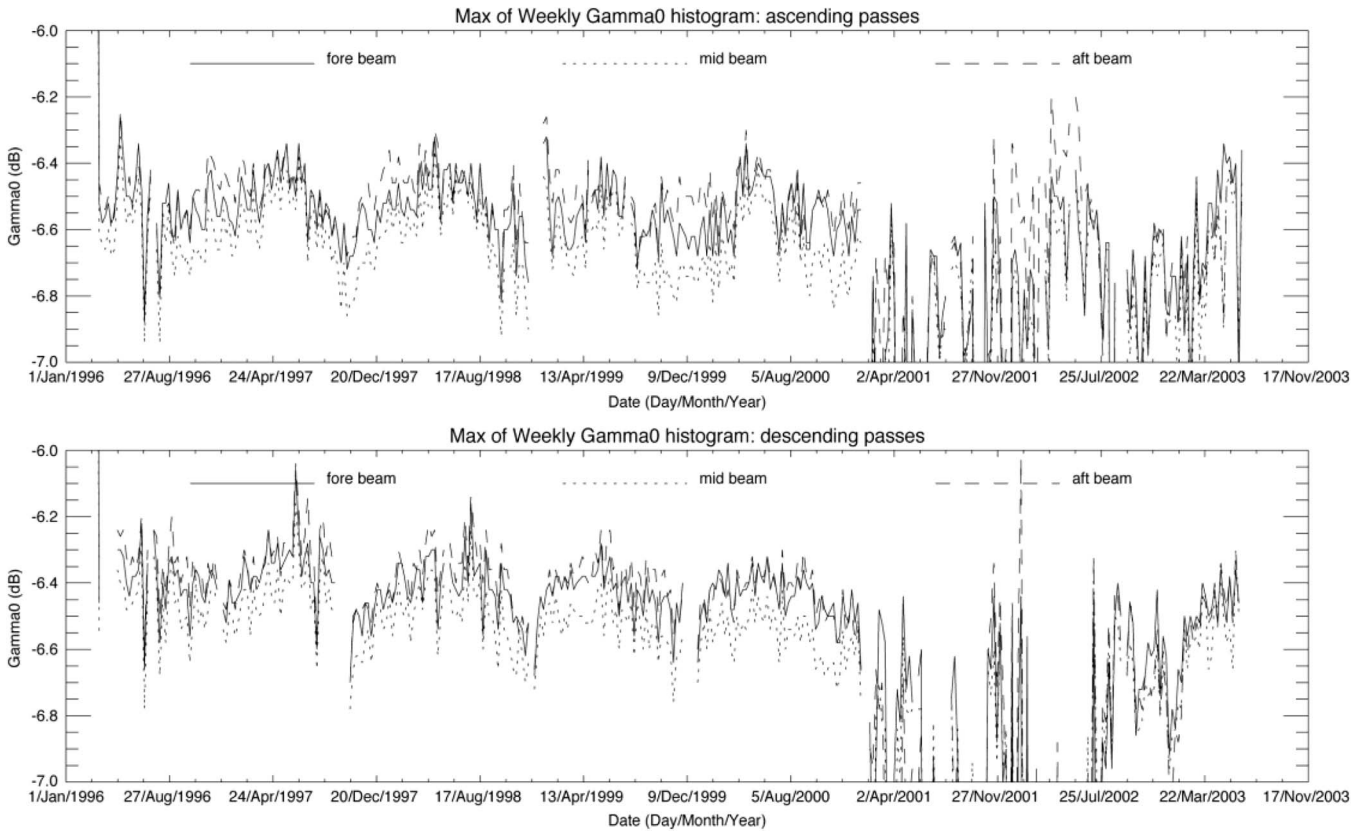
Fig. 7.    Gamma nought monitoring since the beginning of the mission and until the tape recorder failure.
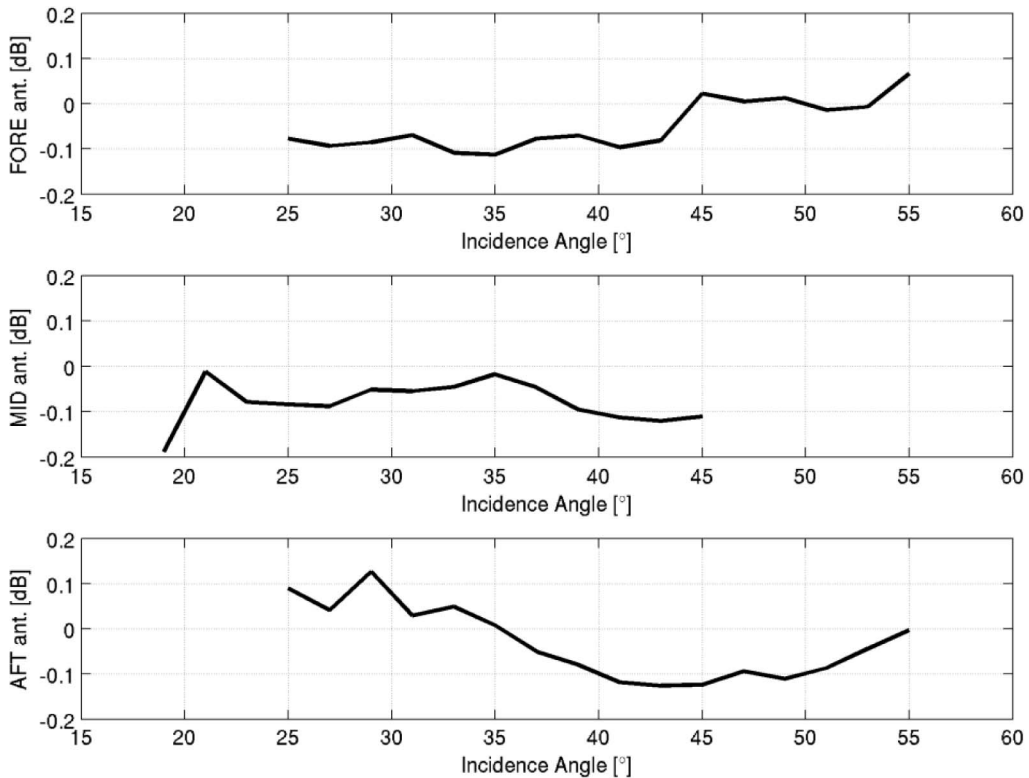


Fig. 8.    Antenna pattern drift between 1996 and 2011 for the ascending overpasses.
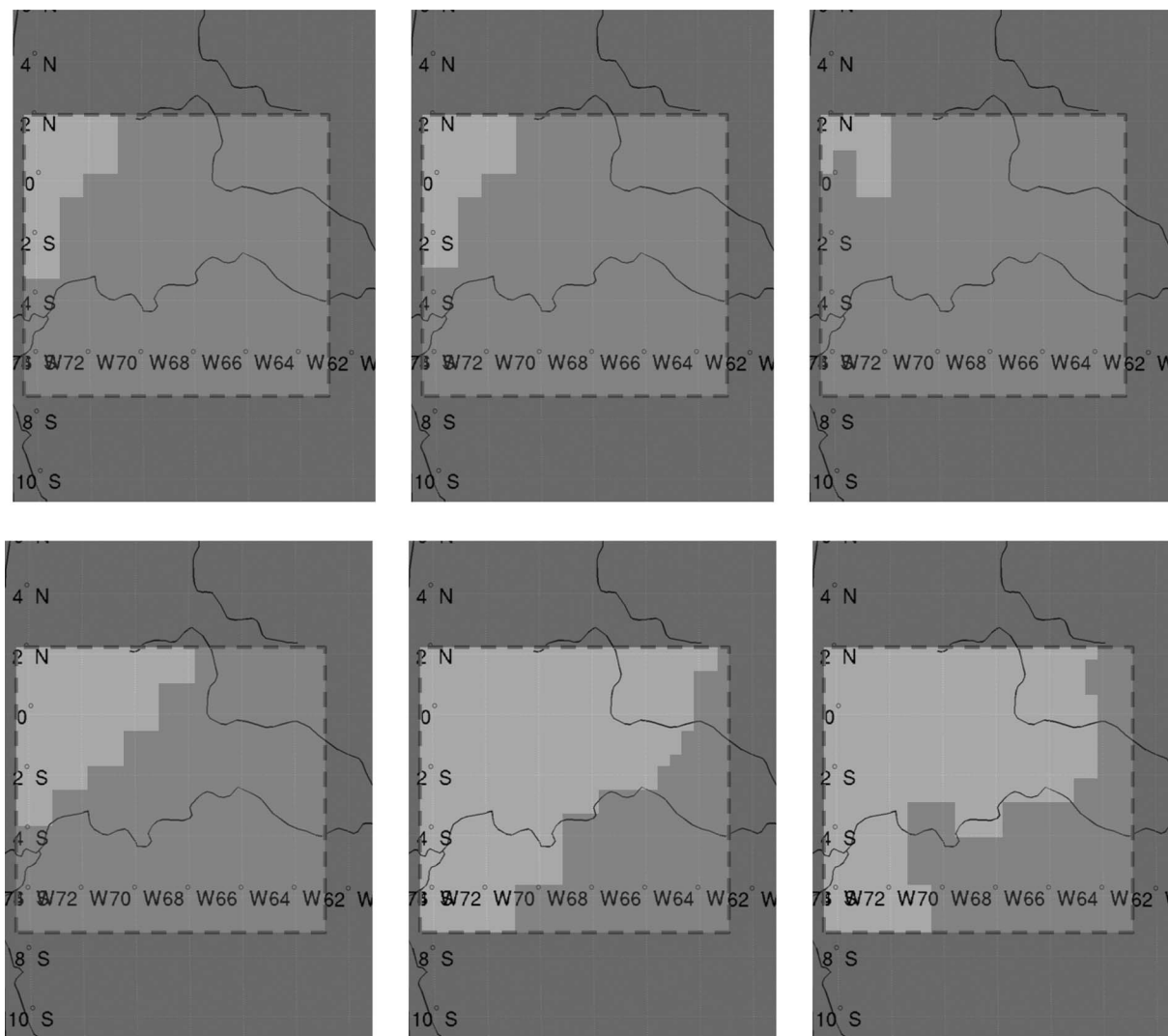
Fig. 9. ERS-2 scatterometer: average $\gamma^0$ over the Brazilian rain forest between January and April 2011 for the (left) fore, (middle) mid, and (right) aft antennas, and for the (top) descending and (bottom) ascending passes. The zone of interest is highlighted; middle gray indicates no coverage.

### A. Rain Forest

Rain forest acts, at the C-band, as a very rough surface, so that the transmitted signal can be assumed to be equally scattered in all directions. Under this assumption, constantly verified and monitored for ERS-2 during the whole mission [7], [8], the measured backscattering only depends on the area observed by the instrument. This purely geometrical dependence can be removed by normalizing the $\sigma^0$ with the cosine of the incidence angle ($\gamma^0$, gamma nought), as expressed in

$$\gamma^0 = P/S^0 = P/\left(S \cdot \cos(\theta)\right) = \sigma^0/\cos(\theta). \quad (3)$$

Gamma nought histograms have been weekly computed by the PCS until the tape recorder failure in 2003. The position of the histogram's peak is shown on the Fig. 7 for the three antennas, for the (top) ascending and (bottom) descending passes. In Fig. 7 the solid lines represent the Fore antenna, the large dashed line the Mid antenna, and the thick dashed line stands for the Aft antenna.

The monitoring shows a very stable instrument calibration within the initial specification (0.5 db) and a geophysical signal with an annual variation of around 0.2 dB. The impact of the ZGM operations is clear visible in the time series from January 2001. In February 2003 a pre-operational version of the ESACA processor was installed in the ground station at Kiruna (S), resuming the nominal performance.

Due to the new Regional Mission Scenario the calibration monitoring activity over the Brazilian rain forest was temporary suspended until October 2007, when, with the inclusion of the Miami and Chetumal ground stations and the consequent improvement of the coverage of the Rain Forest, the monitoring could be resumed. Nevertheless, the poor coverage of the zone does not allow calculating representative statistics.

The possible degradation of the antenna pattern has been also monitored by using the very homogeneous scattering of the Rain Forest. In Fig. 8, the difference (in decibels) between the antenna patterns as measured in 2011 and in 1996 is shown as a function of the incidence angle for the (top) fore, (center) mid, and (bottom) aft antennas. Only ascending overpasses are
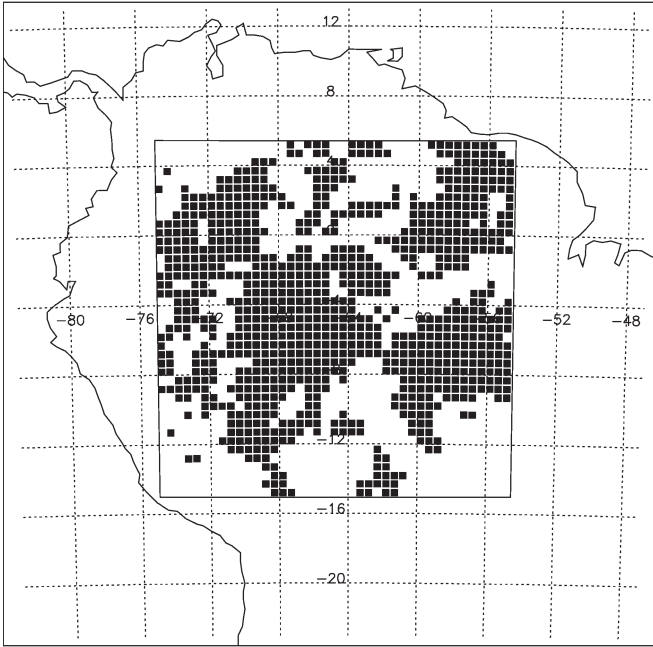
Fig. 10.    Rainforest mask built from ASCAT data.

considered since very poor coverage of that zone is achieved in the descending overpasses, as shown in Fig. 9. Assuming constant and homogeneous scattering from the rain forest, the antenna pattern drift has been calculated by subtracting 2011's acquisitions to the 1996's, as a function of the incidence angle. It is worth to remark that estimations for the 1996 are produced by analyzing one cycle (35 days), while, due to poorer coverage after 2003, for 2011, three cycles have been considered.

In Fig. 9 the zone selected for the calibration monitoring and the coverage achieved are shown for the (left) fore, (middle) mid, and (right) aft antennas as well as the (top) descending and (bottom) ascending passes. The zone of interest is highlighted; middle gray means no coverage in that zone.

*Rain Forest Masking:* Temporal cyclic variations can be observed in the $\gamma^0$ over the rain forest. One-year cycles correspond to seasonal variations. 35-days and single pass cycles correspond to violation of the constant-$\gamma^0$ assumption over the rainforest. It was demonstrated [9] that a spatial masking of particular areas of the rainforest indeed attenuated the single pass cyclic components. The mask is built by excluding areas having a very low or a very high $\gamma^0$ and areas where the $\gamma^0$ exhibits a high variance. The obtained spatial mask actually masks rivers and deforested (urban) areas and favors areas with a homogeneous vegetation type. The mask thus gives a geophysical meaning to the removal of the cyclic components in the $\gamma^0$ results.

Fig. 10 shows this mask (it is here obtained using ASCAT data as due to the partial coverage of the rain forest since 2003, it is not possible to build a complete mask using ERS data).

Fig. 11(a) and (b) shows the $\gamma^0$ pattern over the Amazon rainforest as a function of incidence angle during December 2008 for the ascending and descending passes, respectively. The only relevant (considered) data are from mid/aft antennas in ascending pass and the aft in descending pass. The side antennas still behave approximately as in the global mission

with a lower level. The fore beam is not displayed for the case of selecting only ascending passes because of the poor coverage achieved in the Regional Mission scenario. This does not allow a proper estimation of the Gamma nought as a function of the incidence angle; the same problem has been found for the cross-calibration with ASCAT (see Fig. 21 and Table II).

*B. Polar Regions*

Since the rainforest is not anymore entirely covered by ERS-2, only the monitoring of the fore beam during the descending passes and the mid and aft beams during the ascending passes is possible, with very low statistics. The polar (ice covered) regions were investigated for calibration. Few calibration sites were identified as stable regions (low standard deviation) [5] in Greenland, Arctic sea and Antarctic.

Calibration over ice can be based on two methods: the first method is based on a linear model of the backscatter (in decibels) as a function of the incidence angle. The second method is based on the ice line model which is applicable on sea ice.

*1) Arctic Sea Ice:* Cross sections in the 3-D measurement space reveal that backscatter triplets measured on ice lie on a straight line [10]. This indicates that one geophysical parameter, called ice age, determines the isotropic scattering from ice. The sea ice model [10] initially developed to discriminate between sea and ice backscatter triplets can be used for calibration. For each node (incidence angle), an ice line is determined. The slope and the origin of the line depend only on the incidence angle. The calibration using this model consists in the evaluation of the deviance of the measured backscatter from the ice line model

$$\sigma^0_{calib} = \sigma^0_{meas} - \sigma^0_{theo} \qquad (4)$$

where the theoretical backscatter is defined as follows:

$$\sigma^0_{theo}(\theta, a) = \sigma^0_{theo}(\theta) + a e_a. \qquad (5)$$

with $e_a$ the slope and $\sigma^0_{theo}(\theta)$ the offset. A result of the application of the ice line model is shown in Fig. 12(a) and (b), the bias of the measured $\sigma^0$ is compared to the theoretical one during December 2008 for the ascending and descending passes.

*2) Greenland:* Fig. 13 shows the variance of $\sigma^0$ over Greenland (node 10) for the three beams. The central part of Greenland is found to be a stable area.

The linear approximation assumes that the backscatter has a linear dependence on incidence angle. Therefore, it can be modeled as a linear function of the incidence angle [11]

$$\sigma^0(\theta) = A + B(\theta - 40°) \qquad (6)$$

where $A$ is the 40 ° normalized backscatter.

The area of interest is divided in number of cells. The $\sigma^0$ and incidence angles are accumulated for a given period of time in each cell. A line is fitted to these measurements. The slope of the line is determined for each cell. All the backscatter is normalized to $\sigma^0(40°)$ i.e., the backscatter at 40° is taken as a reference.
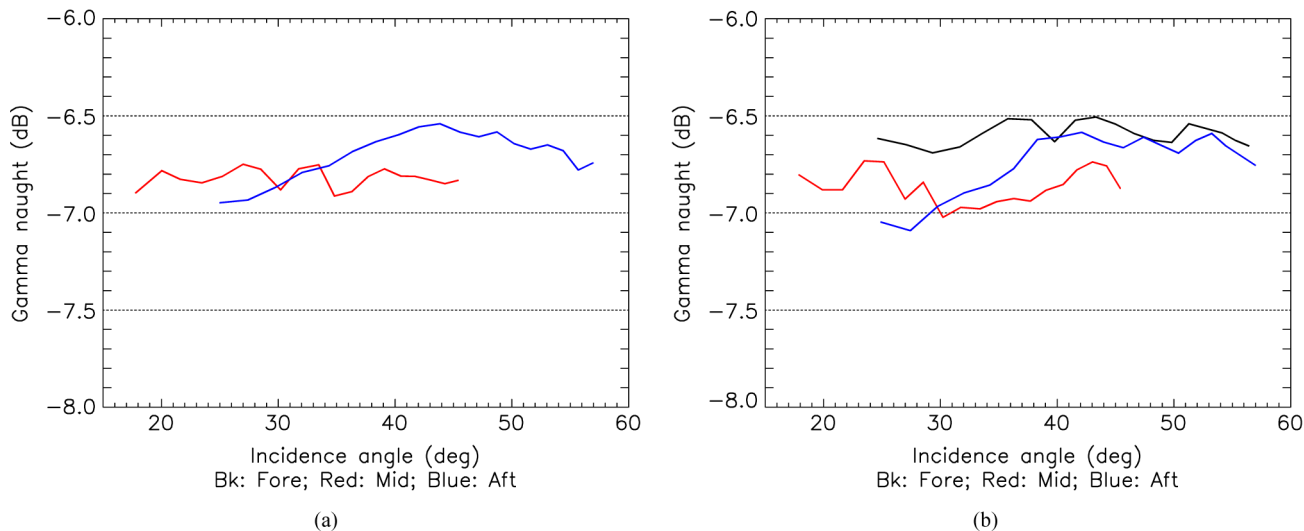
Fig. 11.   Rainforest calibration for (a) ascending and (b) descending passes.

TABLE  II
SUMMARY OF THE CROSS-CALIBRATION METHODS

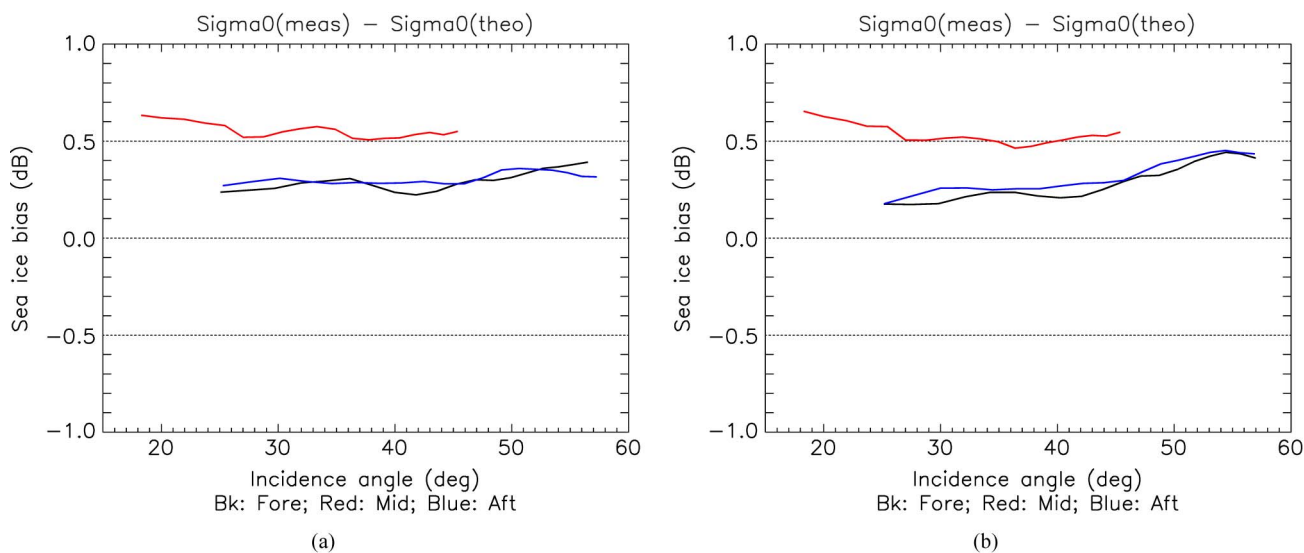| Method /Beam | Standard Deviation | | | Mean value | | |
|---|---|---|---|---|---|---|
| | Fore | Mid | Aft | Fore | Mid | Aft |
| Sea ice cross-calibration | 0.022 | 0.018 | 0.022 | 0.13 | 0.09 | 0.14 |
| Rainforest cross-calibration | - | 0.075 | 0.037 | - | 0.23 | -0.01 |
| Ocean cross-calibration | 0.091 | 0.068 | 0.073 | 0.15 | 0.12 | 0.13 |
| Collocation cross-calibration | 0.097 | 0.070 | 0.095 | 0.25 | 0.12 | 0.33 |



Fig. 12.   Ice calibration for (a) ascending and (b) descending passes.

Fig. 14 shows the $\sigma^0(40°)$ values corresponding to December 2008. The evolution of this $\sigma^0(40°)$ could be monitored by computing the same value over a long period of time at a given location. A $\sigma^0(40°)$ time series for a period of 15 months since November 2008 is shown in Fig. 15.

## C.  Ocean Calibration

In order to monitor the antenna pattern over the ocean, numerical weather prediction (NWP)-based ocean calibration method can be used to compute the difference between the mean measured backscatter and the simulated
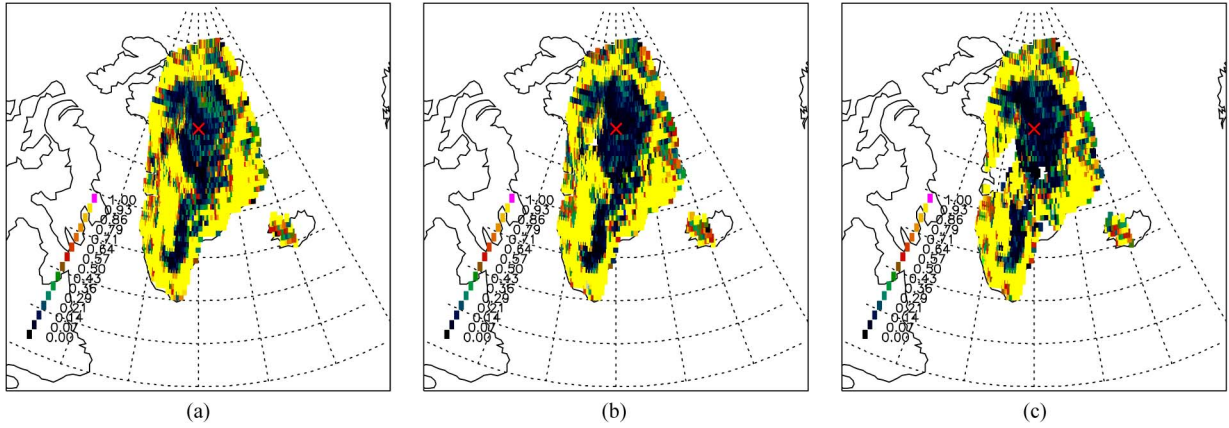
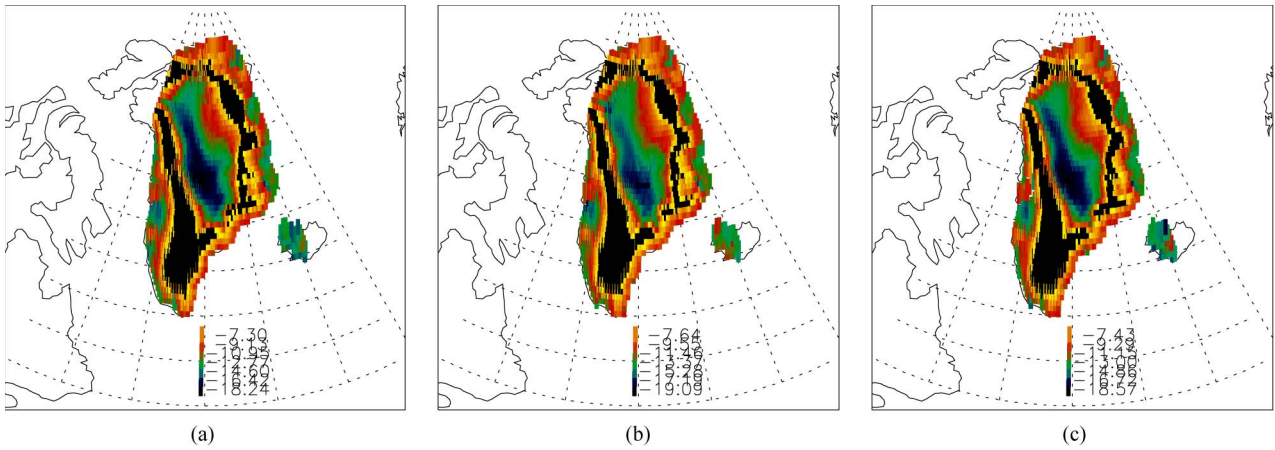Fig. 13.   Variance of the $\sigma^0$ over Greenland for the (a) fore, (b) mid, and (c) aft antennas.



Fig. 14.   $\sigma^0(40°)$ over Greenland for the (a) fore, (b) mid, and (c) aft antennas.

backscatter using collocated NWP winds and a geophysical model function (GMF).

The data are binned into wind speed and direction bins of respectively 2 m/s and 10 deg. The $\sigma^0$ are accumulated in the corresponding bins depending on the collocated NWP wind, for each node and beam. The $\sigma^0$ is averaged over the wind direction and then over wind speed. Weighting of the $\sigma^0$ is used to compensate an eventual nonuniformity of the wind direction distribution. The smallest wind speed bin is discarded from the average. Given the limited coverage of ERS-2, the ocean calibration is mainly performed on the northern Atlantic Ocean.

The average $\sigma^0$ bias compared to the simulated $\sigma^0$ during December 2008 is displayed in Fig. 16(a) and (b) for the ascending and descending passes, respectively.

In general, the patterns are comparable to the patterns produced during the global mission. There is a large negative bias at high incidence angles, and high bias at near range, which disappears when the CMOD4 GMF is used (not shown). The gap between the for/aft and the mid beam is slightly larger in ascending than descending pass. On the other hand, the gap between fore and aft antennas is wider in descending pass.

### D. Cross-Calibration With ASCAT

ERS-2 and METOP-A scatterometers are very similar instruments. They are both active, real aperture C-band radars. They measure (ERS-2 since 1995 and METOP-A since 2006) the global normalized radar cross-section.

Long term studies need data acquired during several years, which requires continuity and stability of the instruments. Moreover, simultaneous assimilation of ERS-2 and METOP-A data requires consistency. Hence, a cross-comparison of the measurements is essential.

A major issue in cross-comparison is the impossibility to perform direct comparisons of the $\sigma^0$ due to the lack of collocated simultaneous measurements performed using exactly the same acquisition geometry (incidence angle, look angle). In order to cope with this, models are used to bridge these differences. The models and the related assumptions are typically only valid over particular areas at the surface of the Earth. And what results is the extraction of a geophysical quantity (or a bias with respect to a modeled geophysical quantity). These biases can then be compared between different instruments.

Four distributed targets (rain forest, ocean, sea-ice, and collocated measurements) and associated models are considered and described below.
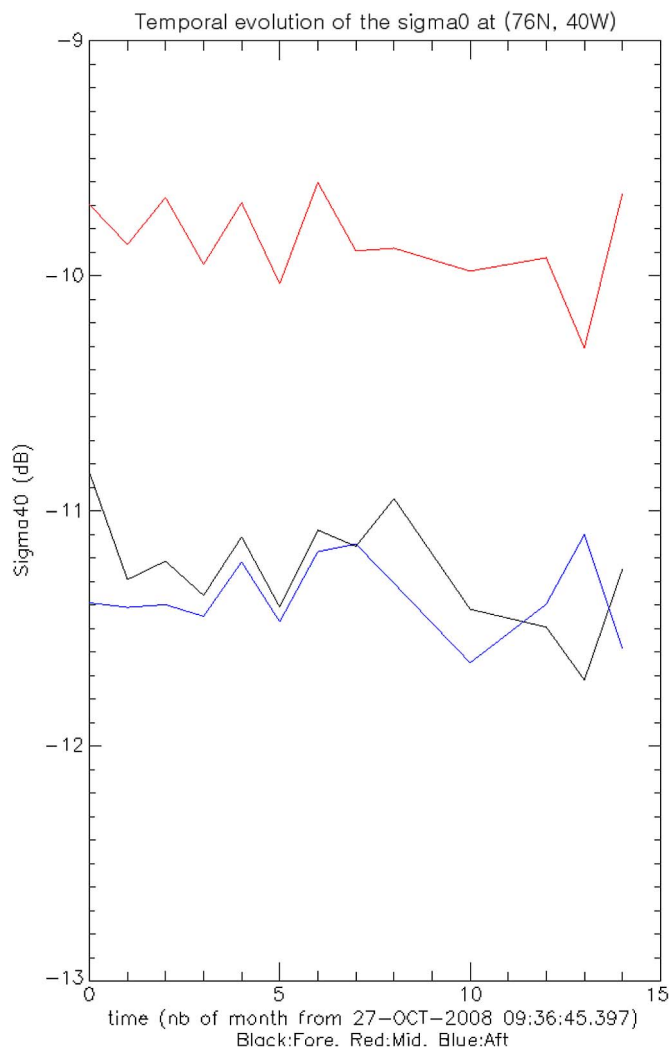
Fig. 15.    Evolution of the $\sigma^0(40°)$ over 15 months since Nov. 2008.

A central assumption is that biases between the instruments would be independent of the amplitude of the sigma nought, and possibly incidence-angle dependent as they would be attributed to varying elevation antenna gain.

*1) Rain Forest:*  The isotropy assumption over the rain forest and its assumed temporal and spatial stability lead to the constant $\gamma$ model obviously only valid over the rain forest. A constant $\gamma^0$ of 6.5 dB is assumed as model and the bias as a function of the incidence angle w.r.t. that model is considered. A comparison of the biases permits a meaningful comparison of the instruments.

Fig. 17 shows the mean $\gamma^0$ pattern (to which 6.5 dB has been added) of the two instruments and their difference over the common incidence angle range, namely solid red line is for ERS-2, blue for ASCAT, and black for their difference, the dashed lines represent plus/minus the standard deviation associated to the mean $\gamma^0$. The pattern of ERS-2 exhibits a high variance due to low number of samples and the fact that ERS-2 covers only a small part of the rainforest.

*2) Sea Ice:*  The generalized form of the sea ice model [10] is used, and the data acquired over the Arctic sea ice during December 2008 are considered. The ice flag present in the

ERS-2 product is used to reject open water areas. Selecting only the $\sigma_0$ values with a distance to the ice model lower than 1 dB, the sea ice calibration method described above is applied on the data from both scatterometers separately, where the ice age parameter is obtained from the ERS-2 data. This yields a model bias for each instrument, and these model biases are then compared over the common incidence angle range. As for Fig. 17, Fig. 18 shows the model bias of the two instruments and the difference between them. Solid lines are for the mean value and dashed lines for the standard deviation; red is for ERS-2, blue for ASCAT, and black for their difference.

*3) Ocean:*  The ocean calibration method described in the last paragraph is applied on both scatterometers data separately. This yields a model bias for each instrument, and these model biases are then compared over the common incidence angle range. A small area ([20 N–60 N], [80 W–0 E]) in the Northern Atlantic Ocean is taken into account in order to have data covering the same region and thus remove differences due to the different coverage of both instruments. The data considered are from December 2008, and the CMOD5 GMF is used.

Fig. 19 shows the model bias and the bias for the two instruments. In Fig. 19, solid lines are for the mean value and dashed lines for the standard deviation; red is for ERS-2, blue for ASCAT, and black for their difference. A dramatic increase (up to 1 dB) of the model bias at high incidence angles for the two instruments and all the antennas can be noticed. This is believed to be an artifact of the GMF. On the other hand, there is a sharp increase at low incidence angles. These patterns at the swath edges are in fact noticeable in the two previous methods (RF and ice) with lower amplitude, while they are exacerbated (probably by the GMF) in the ocean calibration. The bias is on average positive, except at a certain incidence angle between 40 and 50. We notice that the bias is negative at the same incidence angle ranges as the $\gamma^0$ bias (see Fig. 17).

*4) Co-Location:*  If collocation requirements are relaxed, a small number of collocated measurements in time, space, and geometry can be found. The maximum difference considered in time, distance, incidence angle, and azimuth angle are respectively 1 h, 12.5 km, 1 deg, and 5 deg. The average of the $\sigma^0$ difference is computed for each incidence angle over the common range of incidence angle. This is done for ascending and descending passes separately.

Fig. 20 shows the bias between ASCAT and ERS-2 scatterometer for ascending passes. The result shows clearly that the backscatter measured by ASCAT is higher by around 0.2 dB. The same result was obtained for the descending passes (not shown). As it was stated in the results of ice and ocean calibration, the side antenna bias is larger than the midantenna.

*5) Comparison of the Methods:*  The biases from the four cross-calibration methods are plotted together in Fig. 21, solid lines stand for the mean value, while the dashed lines represent the standard deviation. Black is for ice calibration, red for the sigma nought calibration, blue for the ocean calibration, and green for the rain forest calibration. As for Fig. 11, rain forest calibration cannot be calculated the fore beam/ascending passes, due to the poor coverage of ERS-2 during the Regional Mission Scenario.
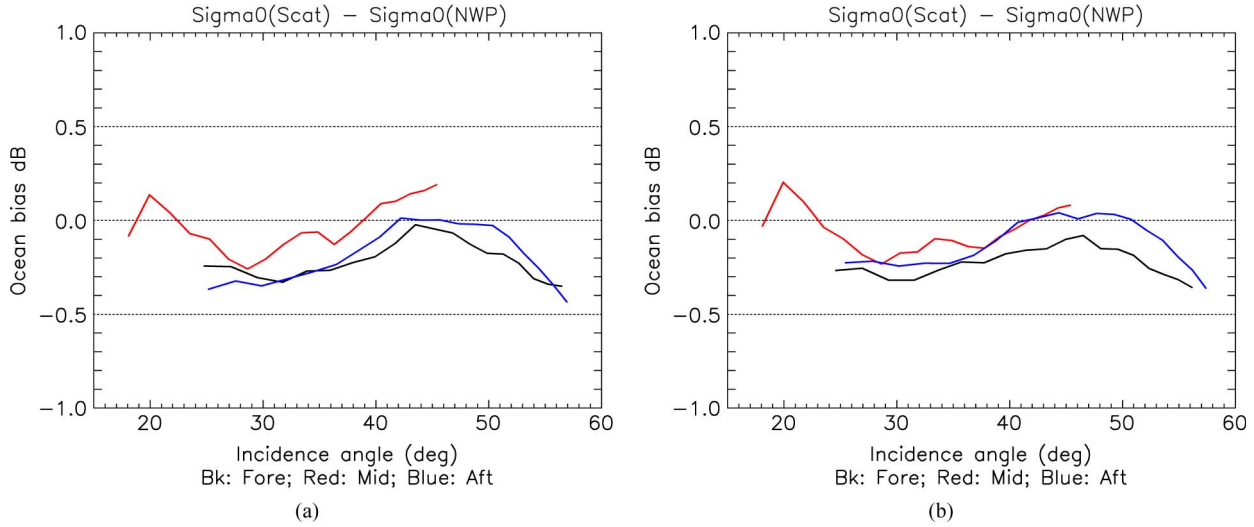
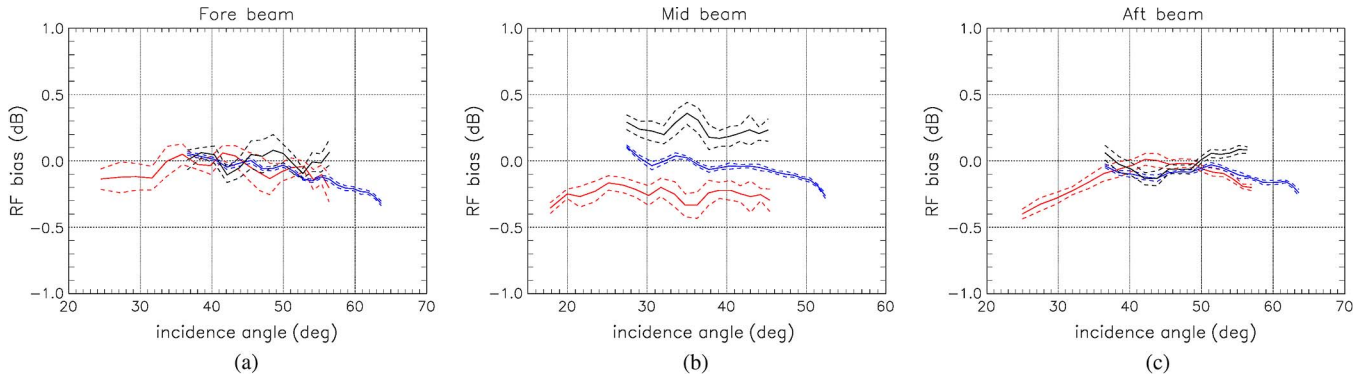Fig. 16.   Ocean calibration for (a) ascending and (b) descending passes.



Fig. 17.   Cross-comparison over the Amazon Rainforest during December 2008 for the (a) fore, (b) mid, and (c) aft antennas. Red lines are for ERS-2, blue for ASCAT, and black for their difference, solid and dashed lines indicate mean value and standard deviation, respectively.



Fig. 18.   Cross-comparison over the sea ice during December 2008 for the (a) fore, (b) mid, and (c) aft antennas. Red lines are for ERS-2, blue for ASCAT, and black for their difference, solid and dashed lines indicate mean value and standard deviation, respectively.
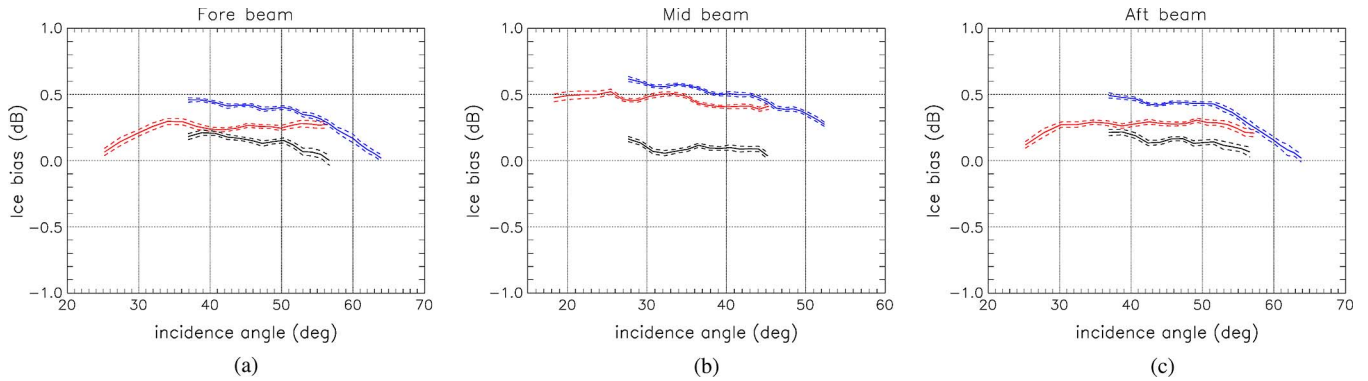
Discrepancies between the four methods can be noticed, though generally, all the biases are positive. Given these differences between biases, the methods need to be assessed and ranked. The assessment criterion chosen is the variability of the method. The evaluation of the variability is based on the variance.

As a summary of the section, the results for all the cross-calibration methods are shown in Table II, where the mean value and the standard deviation of this bias averaged over the incidence angles (as presented in the previous sections) are shown for the ascending passes. The methods are ranked by increasing standard deviation.

For all methods (except the rainforest), the standard deviation and the bias of the mid beam are lower than the side beams. On average, the lowest bias/std is obtained by cross-calibration over sea ice, and the largest is obtained by the collocation
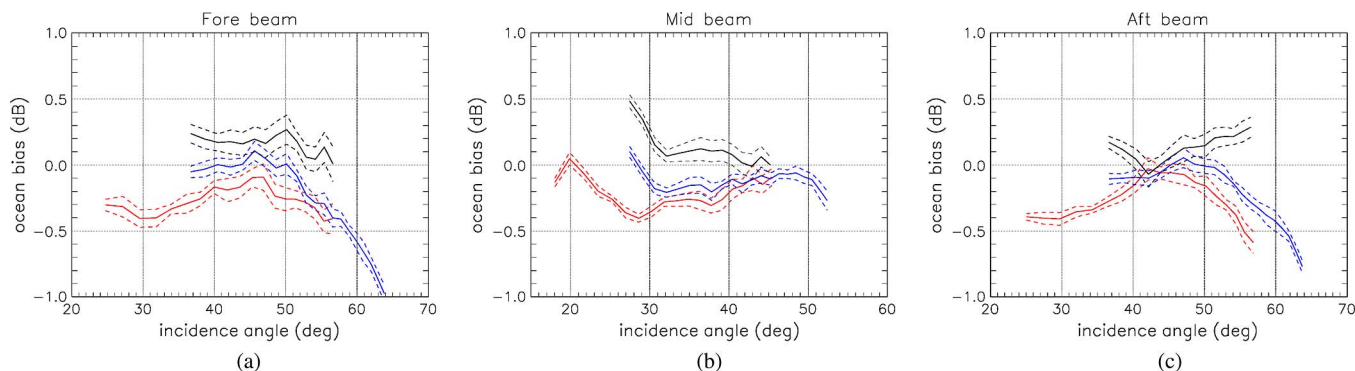
Fig. 19. Cross-comparison over the ocean during December 2008 for the (a) fore, (b) mid, and (c) aft antennas. Red lines are for ERS-2, blue for ASCAT, and black for their difference, solid and dashed lines indicates mean value and standard deviation, respectively.
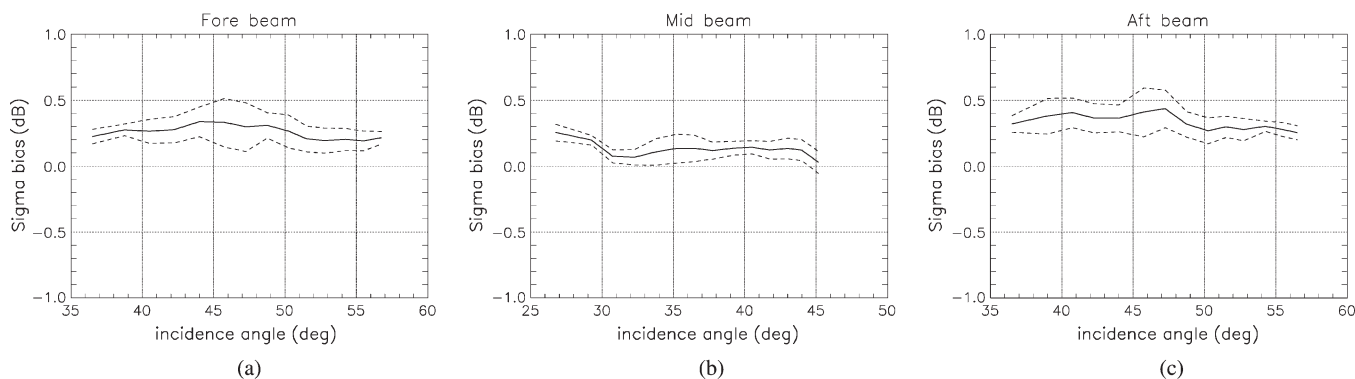


Fig. 20. Colocation cross-comparison for the (a) fore, (b) mid, and (c) aft antennas.

method. It should be pointed out that the rainforest mask and the ice age parameter are retrieved from the data itself. This may contribute in the diminution of the standard deviation. The NWP winds used in the ocean cross-calibration are, instead, external information, independent of the scatterometer data. Another point is that the collocation method includes all type of targets (land, sea and ice). Different bias/std can be obtained by including/excluding different target types.

Finally, although the methods are applied on the same region, the number of samples differs a lot from a method to another, for instance, the collocation method has the smallest data size, which can contribute in increasing or decreasing the standard deviation. The spatial and temporal coverage for each method and the consequent data set are reported in Table III.

Since ERS-2 is operating in regional mission scenario, it covers mainly the Northern hemisphere. Hence, the test area is restricted in order to have the two scatterometers (ERS-2 and ASCAT) covering the same region, and such that the comparison is made using almost the same data size.

The temporal coverage is the same for all methods, except for the cross-calibration over the rainforest. Due to the limited coverage of ERS-2 over the rainforest, three cycles of data are used to get increase the number of measurements, in spite of that, few acquisition are available.

## V. DATA REPROCESSING

In 2003, the GCOS Steering Committee identified the wind speed and direction as two of the ECVs [12] to be monitored in

order to get a better understanding of the long-term and scale phenomena affecting the global climate.

Within this framework and to create homogeneous, high-radiometric-quality, and high-resolution wind speed and direction databases, the reprocessing of both the ERS-1 and ERS-2 campaigns has been planned, and it is being performed since July 2007.

The main objectives of the ASPS project are:

- Reprocess ERS-2 zero-gyro mode data acquired between 2001 and 2003.
- Reprocess the data acquired in the so-called "Regional Mission Scenario." These data are available only for a small segment in the visibility of each ground stations and different ground stations can acquire data over the same area simultaneously. ASPS software is able to re-process all the data segment available from the different ground stations in one segment, by selecting the best raw data quality from the different stations. This allows an enhanced coverage of the nodes with all the three antenna $\sigma^0$ computed.
- Reprocess ERS-1 data, so to build a homogeneous database involving both satellites.
- Provide yaw correction information.
- Enhance the spatial resolution. With the improved algorithm the return signal is processed to provide backscattering coefficients (and all the geophysical parameters derived) with the nominal spatial resolution of 50 km, but also with an enhanced resolution of 25 km.
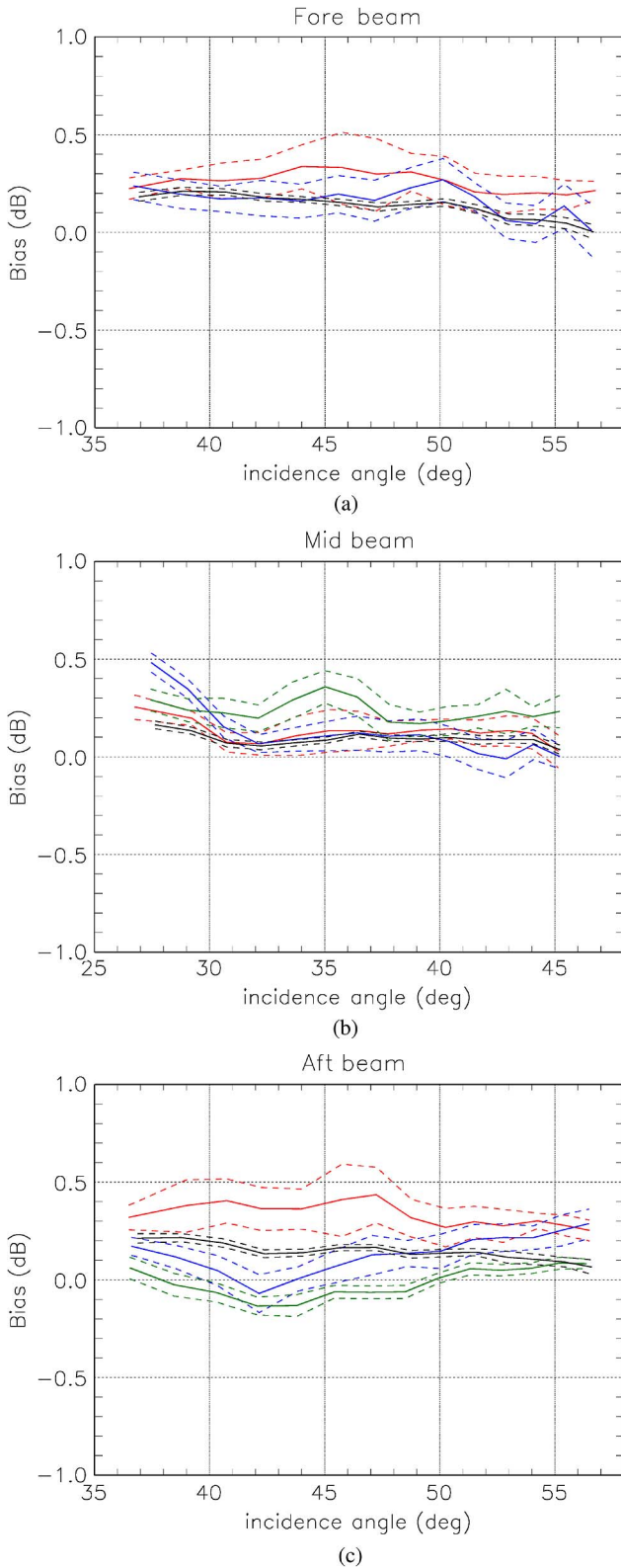
Fig. 21. Comparison of the cross-calibration methods for the (a) fore, (b) mid, and (c) aft antennas. Only ascending passes are shown due to the lack of data for the descending passes.

- Finally, provide a detailed quality control report to monitor the instrument performances and the data quality, including information about:

— Telemetry: Current, voltages, and temperatures, Doppler, yaw, internal calibration, and noise power;
— Level 1: Radiometric stability;
— and Data Processing: Ingestion process, flags statistics, and GMF inversion performance.

To improve the radiometric quality of ASPS scatterometer data, a calibration analysis of the ERS-2 data has been performed with the aim to compute the best calibration constants and evaluate a new improved antenna pattern that has been used in the reprocessing activity. Several modifications have been introduced. Among them, the result obtained during the commissioning was reviewed. Transponder data and rain forest data were reprocessed using TOSCA, and we arrived at the conclusion that, also with the new scatterometer processor, the rain forest data were more stable and more suitable for calibration refinement [9]. The outcome of this activity is a refined gain constant and antenna pattern used in the reprocessing campaign. Apart from that within ASPS, the wind retrieval is performed with the CMOD5N [13] geophysical model derived by ECMWF to compute neutral wind rather than 10-m wind. The main changes between nominal processing and reprocessing are summarized in Table IV.

Currently, a total of 60 cycles (22–81, from May 1997 to May 2003) of ERS-2 have been reprocessed and are available online at [14]. Each reprocessed ASPS data cycle has been submitted to a quality control procedure aimed to verify the completeness of the time series, the correct instrument parameters, the data quality, and the proper processing. The status of the reprocessing campaign is summarized in Fig. 22, where the percentage of missing orbit for each cycle is shown as a bar plot; known problems and unexpected errors are distinguished using brighter and darker grays, respectively.

In addition to the necessity of creating a homogeneous database for wind vectors, ERS-2 reprocessing also permitted the detection of second-order problems that were not identified in the first processing. An example of these is shown in Fig. 23, where the $\gamma^0$ is shown, as estimated during the reprocessing of cycle 71, as a function of the across-track node, for the (top) ascending and (bottom) descending overpasses for the (solid line) for, (dashed line) mid, and (dotted line) aft antennas. It is worth to remind that in the reprocessing the rain forest is also used to monitor the performances of the instrument. In this case, for example, despite a refined (including rain forest measurements) antenna pattern is used, an unusual behavior has been found, as shown in Fig. 23.

As can be noticed, the aft antenna shows very different performance compared to the fore and midantennas; a total of 6 cycles (69–74) proved to be affected by such problem; This analysis has been also confirmed by the Ocean Calibration, so the aft antenna evolution is more related to instrument evolution or configuration rather than change in the observed target. As a consequence of this find, the aft beam antenna pattern for those specific cycles will be recomputed and the new, more accurate one, will be used in the reprocessing of the affected cycles, leading to improve the radiometric stability along the full mission and a better retrieved wind vectors for those cycles.

TABLE III
SPATIOTEMPORAL COVERAGE, AND RESULTING DATA SET FOR EACH CROSS-CALIBRATION METHOD

| Method | Test Area | Time Period | Number of Samples |
|---|---|---|---|
| Sea ice cross-calibration | Arctic sea ice [50N-90N, 110W-130E] | From 01/12/2008 To 31/12/2008 | **ERS-2** 501479 **ASCAT** 769909 |
| Rainforest cross-calibration | Amazonas [15S-5N, 75W-55W] | **ERS-2** From 13/10/2008 To 26/01/2009 **ASCAT** From 01/12/2008 To 31/12/2008 | **ERS-2** 10526 **ASCAT** 107517 |
| Ocean cross-calibration | North Atlantic ocean [20N-60N, 80W-0W] | From 01/12/2008 To 31/12/2008 | **ERS-2** 968003 **ASCAT** 1407985 |
| Collocation cross-calibration | All type of targets | From 01/12/2008 To 31/12/2008 | **ERS-2** 29908 **ASCAT** 29908 |

TABLE IV
CONFIGURATION CHANGES BETWEEN NOMINAL PROCESSING AND REPROCESSING

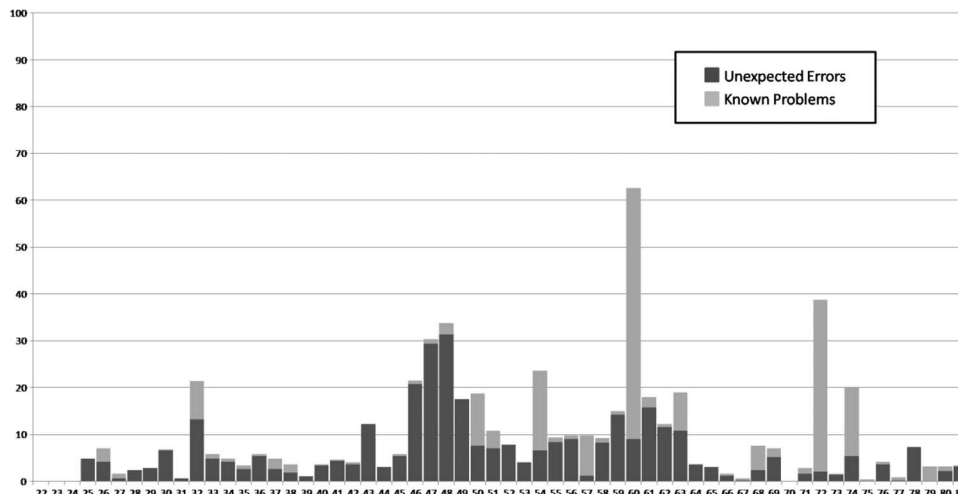| Parameter | Nominal Processing | | Reprocessing |
|---|---|---|---|
| Yaw Angle Estimation | Gyroscopes | | Yaw angle correction using Doppler Compensation |
| | Nominal | 11/1995 – 01/2000 | |
| | Mono-Gyro | 01/2000 – 01/2001 | |
| | Zero-Gyro | 01/2001 – 05/2003 | |
| | Zero-Gyro + Corrected Yaw | 05/2003 – 07/2011 | |
| Sigma Nought Computation | Nominal | 11/1995 – 08/2003 | Improved |
| | Improved (reduce the effect of small data gaps) | 08/2003 – 07/2011 | |
| Kp Computation | Nominal | 11/1995 – 08/2003 | Improved |
| | Improved (echo samples used instead of LUTs) | 08/2003 – 07/2011 | |
| Wind Retrieval Algorithm | CMOD-4 | | CMOD-5N |
| Ambiguity Removal Algorithm | Nominal | 11/1995 – 08/2003 | Improved |
| | Improved (improved handling of the meteo files and implementation of the MSC – Modified Successinve Corrections – algorithm, instead of the CREO algorithm) | 08/2003 – 03/2011 | |
| Antenna Pattern | Nominal (estimated during the commissioning phase using transponders and rain forest) | | Refined (estimated using the rain forest) |

Fig. 22.   Percentage of missing orbit for each cycle. Brighter and darker grays indicate known problems and unexpected errors, respectively.
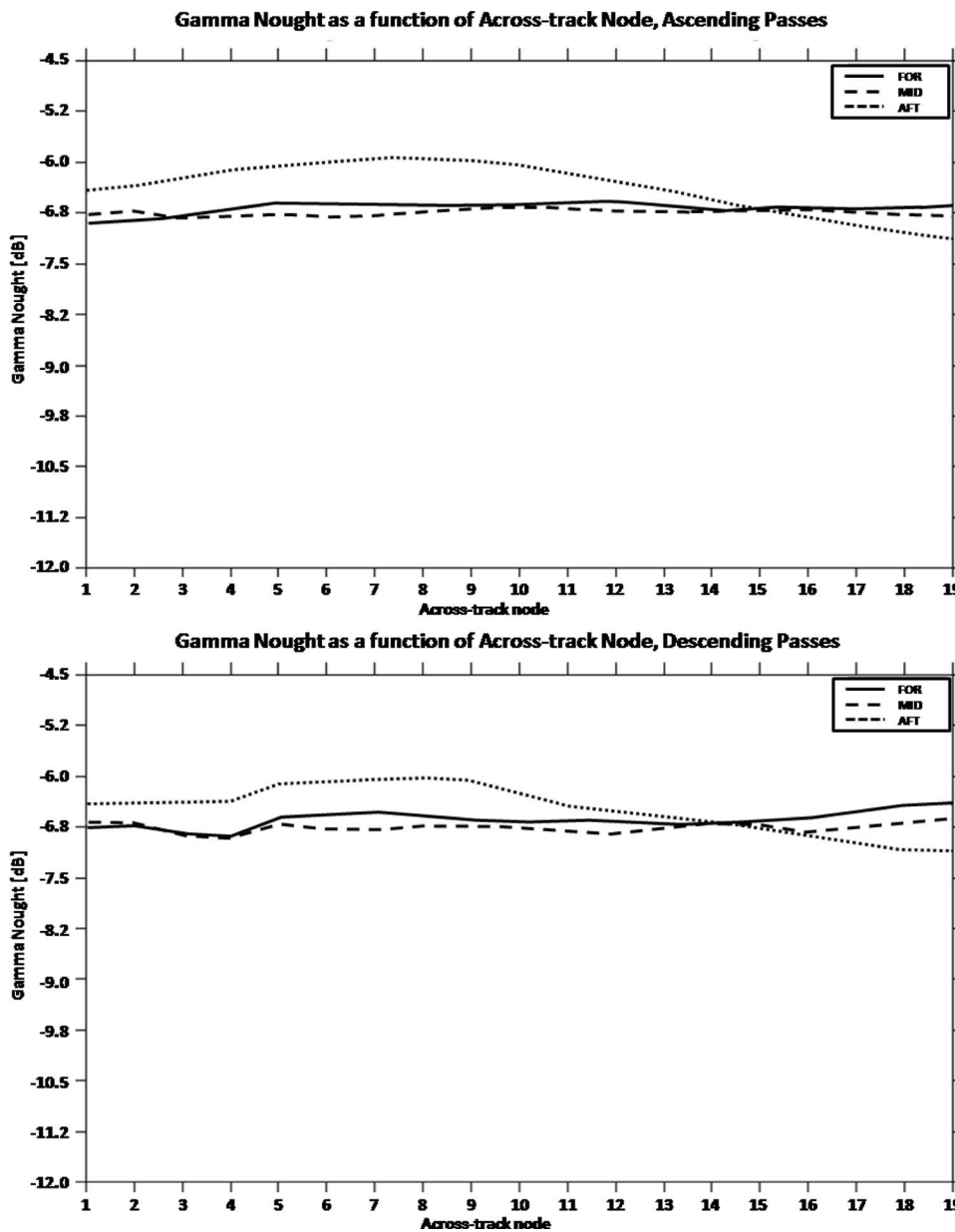


Fig. 23.   Gamma nought as a function of the across-track node for (top) the ascending and (bottom) descending passes.

## VI. CONCLUSION

The ERS-2 will be decommissioned in July 2011, after 16 years of operation. So far, it has demonstrated outstanding performances, each of its payloads achieving excellent scientific results in particular for the scatterometer instrument for both sea surface [13], [15] and soil moisture [16], [17] applications. In addition to that, data from ERS-2 scatterometer are still assimilated in numerical weather forecast model. The wind scatterometer quality monitoring has been assured by ESA, in collaboration with the ECMWF, the Belgian RMA, and Serco SpA. Analyzing the most important descriptors of the instrument performance, it has been shown how the instrument overcame several hardware failures, as well as how data processing was successfully adapted to those failures. Strategies for scatterometer mission calibration and reprocessing have been presented with the current result achived by this exercise.

The extraordinary duration of the mission, even larger if combined with the former ERS-1, permits the creation of a homogeneous database of wind vectors including the last 20 years, fulfilling the recommendations set by the GCOS Steering Committee in 2003.

## REFERENCES

[1] C. R. Francis, G. Graf, P. G. Edwards, M. McCraig, C. McCarthy, A. Lefebvre, B. Pieper, P. Y. Pouvreau, R. Wall, and F. Weschler, "The ERS-2 spacecraft and its payload," *ESA Bull.*, no. 83, pp. 13–31, Aug. 1995.

[2] P. Lecomte, "The ERS scatterometer instrument and the on-ground processing of its data," in *Proc. ESA—Eumetsat Workshop Emerging Scatterometer*, Noordwijk, The Netherlands, Oct. 5–7, 1998.

[3] X. Neyt, P. Pettiaux, and M. Acheroy, "Scatterometer ground processing review for gyro-less operations," in *Proc. SPIE—Remote Sensing Ocean, Sea Ice Large Water Regions*, Crete, Greece, Sep. 2002, vol. 4880.

[4] K. Sahr, D. White, and A. J. Kimerling, "Geodesic discrete global grid systems," *Cartography Geogr. Inf. Sci.*, vol. 30, no. 2, pp. 121–134, Apr. 2003.

[5] M. Suess, P. Matos, A. Guiterrez, M. Zundo, and M. Martin-Neira, "Processing of SMOS level 1C data onto a discrete global grid," in *Proc. IEEE Int. Geosci. Remote Sens. Symp.*, Anchorage, AK, Sep. 2004, vol. 3, pp. 1914–1917.

[6] F. Aidt, "Architectural and detailed design document for the wind scatterometer calibration software," ESRIN, Frascati, Italy, Jan. 1990, Tech. Rep.

[7] R. Crapolicchio and P. Lecomte, "On the stability of Amazon Rainforest backscattering during the ERS-2 scatterometer mission lifetime," in *Proc. CEOS SAR Workshop*, Toulouse, France, Oct. 26–29, 1999.

[8] R. K. Hawkins, E. Attema, R. Crapolicchio, P. Lecomte, J. Closa, P. J. Meadows, and S. K. Srivastave, "Stability of amazon backscatter at C-band: Spaceborne results from ERS-1/2 and RADARSAT," in *Proc. CEOS SAR Workshop*, Toulouse, France, Oct. 26–29, 1999.

[9] N. Manise, X. Neyt, and M. Acheroy, "Calibration strategy for ERS scatterometer data reprocessing," in *Proc. SPIE—Remote Sensing Ocean Sea Ice*, Brugge, Belgium, Sep. 2005, vol. 5977.

[10] S. De Haan and A. C. M. Stoffelen, Ice Discrimination Using ERS Scatterometer, SAF/OSI/KNMI/TEC/TN/120. [Online]. Available: http://www.knmi.nl/publications/showAbstract.php?id=344

[11] R. G. Kennett and F. K. Li, "Seasat over-land scatterometer data. Global overview of the Ku-band backscatterer coefficients," *IEEE Trans. Geosci. Remote Sens.*, vol. 27, no. 5, pp. 592–605, Sep. 1989.

[12] Global Climate Observing System (GCOS) web-page. [Online]. Available: http://www.wmo.int/pages/prog/gcos/index.php

[13] H. Hersbach, A. Stoffelen, and S. de Haan, "An improved C-band scatterometer ocean geophysical model function: CMOD5," *J. Geophys. Res.*, vol. 112, p. C03006, 2007.

[14] ERS Reprocessed data. [Online]. Available: http://earth.esa.int/object/index.cfm?fobjectid=1451&i_id=52

[15] M. Portabella and A. Stoffelen, "Scatterometer backscatter uncertainty due to wind variability," *IEEE Trans. Geosci. Remote Sens.*, vol. 44, no. 11, pp. 3356–3362, Nov. 2006.

[16] W. Wagner, G. Lemoine, M. Borgeaud, and H. Rott, "A study of vegetation cover effects on ERS scatterometer data," *IEEE Trans. Geosci. Remote Sens.*, vol. 37, no. 2, pp. 938–948, Mar. 1999.

[17] W. Wagner and K. Scipal, "Large-scale soil moisture mapping in western Africa using the ERS scatterometer," *IEEE Trans. Geosci. Remote Sens.*, vol. 38, no. 4, pp. 1777–1782, Jul. 2000.

**Raffaele Crapolicchio** received the Master degree in engineering degree from Sapienza University of Rome, Rome, Italy, in 1994.

In 1995 and 1996, he was a Researcher within the Department of Electronics Engineering, Sapienza University, in the field of polarimetric SAR signal processing and in the retrieval of geophysical parameters from SAR data such as soil moisture, vegetation coverage, land usage classification in the framework of the MAC EUROPE'91 and Shuttle Image Radar SIR-C/SAR-X experiments. Since 1996, he has been working with Serco spa as Scatterometer Instrument Performances Engineer providing engineering support and technical management to the European Space Agency (ESA) for all the activities and projects related to the long-term monitoring of sensor and data performances, instrument calibration, and processing algorithm evolution of the ERS-2 Scatterometer mission. In 2006, he joined the Soil Moisture and Ocean Salinity (SMOS) development project to support the management of the design, development, integration, and testing of the SMOS data processing ground segment (DPGS) with specific focus on the subsystems devoted to data quality control, sensor monitoring, and L1 data processors. Since 2008, he has been a Science Referee for the *Italian Journal of Remote Sensing* and he was tutor of several Ph.D. works in the fields of scatterometry. He is currently an Engineer in the ESA Sensor Performance, Products, and Algorithms Assurance office working on the ERS scatterometer and SMOS mission.

**Giovanna De Chiara** was born in Salerno, Italy, in 1975. She graduated in Marine Environmental Sciences, curriculum in Oceanography (5-year course study), at the "Parthenope" University of Naples, Naples, Italy, in 2002. She received the Ph.D. degree in civil and environmental engineering from the University of Salerno, Salerno, in 2010.

Her thesis work was developed during an internship period at the European Space Agency (ESA-Esrin), Frascati, Italy. From 2003 to 2005, she joined the "climate observatory" of the Institute of Biometeorology (CNR-National Research Council), Florence, Italy, where she collaborated on different projects regarding meteorological hazards and climate changes. In 2006, she was the recipient of a grant from the National Research Institute C.U.G.R.I. (Consorzio Inter-Universitario per la Previsione e Prevenzioned ei Grandi RIschi) where she worked on remote sensing techniques for meteorological and flood risk analysis. From 2007 to 2010, she worked for Serco S.p.A., Frascati, as Remote Sensing Engineer responsible for the quality control of ERS-2 scatterometer data as part of a support contract with the ESA-Esrin. She is currently working at the European Centre for Medium-Range Weather Forecasts (ECMWF), Reading, U.K., on the validation and assimilation of Wind Scatterometer data.

**Anis Elyouncha** received the Master degree in engineering and the postgraduate degree in wireless networks from the Université Libre de Bruxelles, Brussels, Belgium, in 2006 and 2007, respectively.

Since 2008, he has been working at the Royal Military Academy of Belgium as a Research Engineer in radar signal processing. His research interests include scatterometry, calibration, and imaging.

**Pascal Lecomte** studied in Paris Mathematics and Physics and then moved to Brest to do a Diplôme d'Etude Approfondie in Oceanography Physics. After a one-year period in Mauritania and Senegal with the Orstom (former name of the IRD), he joined the IFREMER that had just created the CERSAT, the French Processing and Archiving Facility dedicated to altimetry and scatterometry. He designed the algorithm to process the ERS scatterometer data and after just more than two years joined ESA which was creating the Product Control Service to monitor and improve the quality of the ERS products. Over more than 21 years, he developed a strategy and put it in place for the current Earth Observation Missions, ERS and Envisat. This strategy is being extended into a multimission environment called sensor performance, products, and algorithm and is described in a strategy document. The quality of this work has been recognized worldwide in particular through the quality of the products delivered by ESA. Since the beginning of 2010, he has been based in the newly created ESA Harwell Center, Oxfordshire, U.K., as Head of the ESA Climate Office. In this position, he has an important role in the development of the ESA CCI, and at international level in the CEOS Climate Advisory Group. Pascal is also a member of the CEOS WGClimate and convener of the CSAB.

**Xavier Neyt** received the Master degree in engineering degree (*summa cum laude*) from the Université Libre de Bruxelles (ULB), Brussels, Belgium, in 1994, the Postgraduate degree in signal processing (*summa cum laude*) from the Université de Liège (ULg), Liège, Belgium, in 2004, and the Ph.D. degree in applied science from the Royal Military Academy (RMA), Brussels and the Université de Liège, in 2008.

From 1996 to 1997, he was Visiting Scientist at the French Aerospace Center (ONERA), Palaiseau, France, and in 1999, at the German Aerospace Center (DLR). From 1997 to 1999, he was responsible for the design of the image compression module of the European MSG satellite and in 2000 to 2007, responsible for the redesign of the ground processing of the scatterometer of the European ERS satellite following its gyroscope anomaly. Since 2008, he has been leading the Scatterometer Engineering Support Laboratory for the European Space Agency at the RMA. He is currently Associate Professor at the Communication, Information, Systems and Sensors department of the RMA, Bruxelles, Belgium. His research interests are radar remote sensing, array processing, and bistatic radars.

Dr . Neyt received the Frerichs Award from the ULB and the special IBM Grant from the Belgian National Fund for Scientific Research (NFWO) in 1995. He also serves on the Radar Systems Panel of the IEEE Antenna and Electronic Systems Society. Since then, he has been working as Research Engineer for the RMA, Belgium.

**Alessandra Paciucci** was born in Rome, Italy, in 1971. She received the M.Sc. degree in mathematics from "La Sapienza" University of Rome, Rome, in 1995.

Her research was on artificial intelligence and applied mathematics. She is currently with Serco S.p.A., Frascati, Italy, as Remote Ground Segment Engineer for the European Space Agency's European Space Research INstitute (ESA-ESRIN), Frascati, Italy. Over the last 15 years, she has worked as Remote Sensing Engineer in charge of the quality control of many of the instruments embarked on the ERS-2 satellite, namely the Wind Scatterometer, the Global Ozone Monitoring Experiment (GOME), and the Radar Altimeter. She is currently involved in the support activities to data processors development, in the context of the data quality control.

**Marco Talone** (S'05–M'11) was born in Valmontone, Italy, in 1981. He received the B.Eng. and M.Eng. degrees intelecommunication engineering from "Tor Vergata" University, Rome, Italy, in 2003 and 2006, respectively. In 2005, he worked on the M.Eng. thesis in the Remote Sensing Laboratory, TSC, Polytechnic University of Catalonia, Barcelona, Spain, where he received the Ph.D. degree in signal theory and communications, in 2010.

He is currently with Serco SpA, Frascati, Italy, as Remote Sensing Engineer. His research interests include microwave remote sensing, both active and passive, as well as retrieval methods for geophysical parameter determination from remote sensing observations.

Dr. Talone has served as Reviewer for the *International Journal of Infrared and Millimeter Waves*, the IEEE TRANSACTIONS ON GEOSCIENCE AND REMOTE SENSING, and the IEEE GEOSCIENCE AND REMOTE SENSING LETTERS.